MATHEMATICAL MODELS FOR SELF-ORGANIZATION OF BIOLOGICAL GROUPS

by

Behnam Torabi
M.Sc. Pure Mathematics, Sharif University of Technology, 2007

A Thesis submitted in partial fulfillment
of the requirements for the degree of
Master of Science
in the Department
of
Mathematics

SIMON FRASER UNIVERSITY
Summer 2010

APPROVAL

Name: Behnam Torabi

Degree: Master of Science

Title of Thesis: Mathematical models for self-organization of biological groups

Examining Committee: Dr. Nilima Nigam
Chair

Dr. Razvan Fetecau,
Assistant Professor, Mathematics Department
Simon Fraser University
Senior Supervisor

Dr. Ralf Wittenberg,
Assistant Professor, Mathematics Department
Simon Fraser University
Co-supervisor

Dr. Paul Tupper,
Associate Professor, Mathematics Department
Simon Fraser University
SFU Examiner

Date Approved: August 9, 2010

Declaration of
Partial Copyright Licence

Abstract

It is observed that coherent motions like bird flocks and fish schools are common phenomena in biology. Recently, many mathematical models have been developed in order to understand the mechanisms that lead to such coordinated motions. In this thesis I consider two models based on the Langevin equation with different external forces. In these Lagrangian models the motion of the group is determined by pairwise interactions. For the first model we perform an H-stability analysis, recover a wide range of interesting patterns and study the state transition induced by noise. The second model contains a different interaction potential. We perform a weak noise limit and study the case when the potential has random coefficients. We also derive the continuous versions of the deterministic cases of these models by using statistical mechanical theory.

Keywords: Aggregation; Individual-based and continuum models; Attractive-repulsive potentials; Noise induced transitions.

Acknowledgments

I would like to thank my supervisor Dr. Razvan Fetecau for his patience, teaching, advice, support and to thank Dr. Ralf Wittenberg and Dr. Paul Tupper for their guidance in this thesis. I would also like to thank the Mathematics department's faculty and staff members for helping me during these two years.

Contents

List of Figures

Chapter 1

Collective Motion in Animal Groups

A swarm describes an aggregate of animals of similar size and body orientation, moving as a single coherent entity. Swarm studies can be applied to insects, birds, fish, various microorganisms such as bacteria, and people [3,22,31]. In the last years the aggregation phenomena

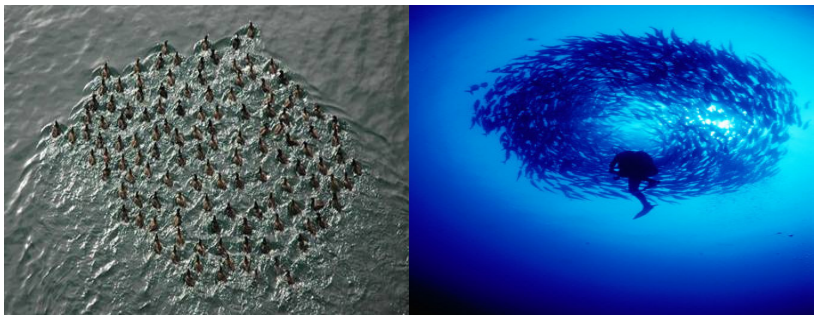

(a) (b)

Figure 1.1: (a) Surf Scoters in English Bay,Vancouver,Canada [44] (b) Diver in the middle of school of fish [50]

on animal groups have received much attention and has become one of the hottest topics in the mathematical biology literature. It is a paradigmatic example of self-organization and grouping behaviour in the absence of centralized control. This mechanism of group formation goes beyond the level of analysis of individuals, because it studies the transition of the local rules for the individuals to a coherent global state. There are many different scales at

which social aggregations can appear, from microscopic populations of cells to macroscopic bird flocks, buffalo herds, insect swarms, and fish schools. Scales of different swarms may vary widely, from $10^{-10}m^2$ in cells and bacteria, spanning up to 10^8m^2 in cross-sectional area for African migratory locust swarms [19]. Groups may also have different dimensionalities, for example the three-dimensional rolling structure formed by the locusts and the two dimensional flat structure of vortex-like ant mills.

There are some interesting advantages of swarming that have been found recently. For example, Oxford university research on locusts [41] has found that swarming behaviour addresses overcrowding. Also, flying in flocks help birds save energy. For instance, flying in a V-formation leads to energy savings which have been estimated in the range $12 - 20\%$ [7]. There are many benefits for fish from schooling behaviour that include better defense against

(a) (b)

Figure 1.2: (a) Swarming locusts [43] (b) A flock of geese flying in a V-formation [45]

predators, enhanced foraging success, better prey detection, and higher success in finding a mate. Swarm behaviour also emerges in groups of people, such as soldiers swarming over parapets. In Cologne, Germany, two biologists from the University of Leeds [48], demonstrated a flock-like behaviour in humans. The behavioural pattern of people has similarities with that of a flock, in which a change in direction of five percent of the group will result in the whole group to follow. If everyone were distanced from one person, called predator, the flock behaved very much like a school of fish.

There are also some disadvantages to being in a group, primarily through increased competition for resources. Competing influences of selective cost and advantage conferred by

the aggregate determines the size of the group during time evolution. The most interesting situations, and even surprising, in swarming is where no "leader" with specific properties is present in the group and interactions are short-range [34,38].

One of the primary tools for exploring the connection between individual properties and group properties is mathematical models. These models enable researchers to test sets of interaction mechanisms and visualize the resulting group behaviour which are generally not directly predictable from the rules alone.

In their simplest and most general form, the mathematical models of animal swarms represent individual animals that follow three rules: (i) move in the same direction as the neighbours, (ii) stay close to neighbours, (iii) avoid hitting neighbours. Variations on these rules are used in different models. These are usually implemented by considering concentric "zones" around each individual as follows [6,12,13,42]:

1. Zone of Repulsion: a close region around the individual that causes other individuals to move away once they get into this region, due to its closeness to the individual.

2. Zone of Alignment: a close region contain the zone of repulsion with in which the individuals seek to align its direction of motion with its neighbours.

3. Zone of Attraction: a larger region extends as far away from the individual as it is able to sense; the individual will seek to move towards a neighbour.

Note that the models usually produce motion that "looks like" that of a swarm of locusts, a school of fish, or a flock of birds, but the similarities are difficult to quantify and therefore the models mostly do not provide clear predictive power [32,40].

There are two types of mathematical models for collective motions, Lagrangian and Eulerian models [9,17,20,27]. Tracking positions and velocities of individuals forms the essence of Lagrangian models. This is in contrast with Eulerian models where the local flux of individuals via population density is used.

The Lagrangian models consist of high dimensional coupled ordinary differential equations (ODEs), whereas Eulerian models are described in terms of advection-diffusion partial differential equations (PDEs) [1,21,24, 27]. Eulerian models correspond better to very large

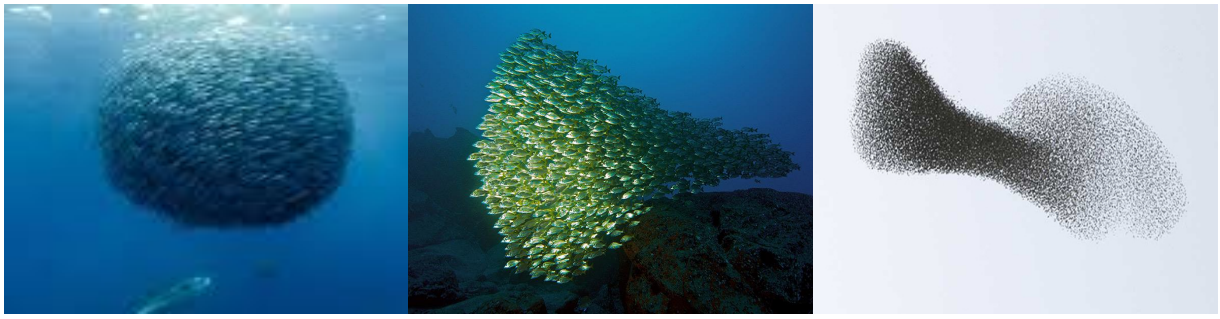

(a) (b) (c)

Figure 1.3: (a) A school of fish swimming in spherical formation [49] (b) A 3-dimensional fish school [47] (c) Starling swarming [46]

populations (insects, bacteria, etc.), while Lagrangian models better describe smaller groups with distinguishable individuals. Indeed, by an Eulerian approach some important aspects of the dynamics may be omitted [26].

The stochastic versions of Lagrangian models, under suitable approximations, may lead to Eulerian models which are easier for analysis in many cases using tools of partial differential equations [8,17]. But Lagrangian models contain more information about individuals, at the expense of analytical difficulty due to their high dimension.

From the ecological point of view the dynamics of "group properties", such as population density, are more important descriptions of aggregated spatial distributions compared to individual movements and positions [17]. However, in many situations where a continuous description of the swarm is not appropriate (e.g., when the number of organisms in the swarm is small), then the Lagrangian approach, following the coordinates of individuals is preferable [25,36].

The numerous interactions between the individual units increase the complexity of Lagrangian models. While the interactions may be relatively simple, some feedbacks are created by a complicated network of interactions in the system. These feedbacks make the emergent group properties difficult to predict. We note that in order to simplify the system

of equations of motion, some assumptions are made which are not very realistic. For example, one of the most important assumptions is that individual members of a population are considered identical. In general this not the case, as individuals are unique and characterized by variables such as age, size, fertility, internal structure, etc. A typical Lagrangian model is based on the Newtonian mechanics equations of motion with acceleration, frictional drag, and a variety of forces causing net motion, alignment, velocity matching, as well as mutual interactions [25].

The study of swarms is also important from the application point of view; multi-robot systems may be used in underwater or space exploration missions, or for the completion of military and other dangerous tasks, such as land-mine detection and removal or earthquake recovery [2]. Additionally the swarm study has strong impact on ecology: fish schools have been very efficiently exploited by fishers, sometimes leading to extinction.

In Chapter 2, we consider the model

$$\frac{d\mathbf{x}_i}{dt} = \mathbf{v}_i, \qquad m_i \frac{d\mathbf{v}_i}{dt} = \alpha \mathbf{v}_i - \beta |\mathbf{v}_i|^2 \mathbf{v}_i - \nabla U_i$$

which we will call model I. Here, $\mathbf{x}_i$ and $\mathbf{v}_i$ are the position and velocity of the individual i with mass m_i. The third term on the right hand side of the $\mathbf{v}_i$ equation is the external force; and U_i is an interaction potential which depends only on the positions $\mathbf{x}_i$. In this chapter we do some stability analysis and will explore how rules and interactions at the individual level lead to some interesting patterns at the group level. Various aggregation geometries will be presented and we explore a state transition from translational motion to rotational motion.

In Chapter 3, we study a Lagrangian model of N self-propelled particles of the form

$$\frac{d\mathbf{x}_i}{dt} = \mathbf{v}_i, \qquad m \frac{d\mathbf{v}_i}{dt} = F_i(\mathbf{v}_i) - \omega^2(\mathbf{x}_i - \mathbf{R}(t)) + \xi_i(t)$$

which we call model II. Here, $\mathbf{x}_i$ and $\mathbf{v}_i$ are the position and velocity of particle i with mass m, F_i is the dissipative force and $\mathbf{R}(t)$ is the position of the center of mass at time t. This model includes stochastic forces, $\xi_i(t)$, and considers fluctuations in the behaviour of individuals. Following [15] we discuss the weak noise limit and conclude that in the weak noise limit the longitudinal dispersion of the swarm, along the direction of its translational motion,

is much smaller than its orthogonal dispersion. We also derive new solutions for a different potential, scaling the diameter of some solutions and end up with a transition behaviour.

In chapter 4 we present, using methods from statistical mechanics, the derivation of the continuum versions of the deterministic cases of the above models. The continuum equations corresponding to model II are

$$\frac{\partial \rho}{\partial t} + \nabla \cdot (\rho \mathbf{u}) = 0,$$
$$\frac{\partial \mathbf{u}}{\partial t} + \mathbf{u} \cdot \nabla \mathbf{u} = \alpha \mathbf{u} - \beta |\mathbf{u}|^2 \mathbf{u} - \frac{1}{m^2} \nabla \int_{R^d} V(\mathbf{x} - \mathbf{y}) \rho(\mathbf{y}; t) d\mathbf{y}.$$

Here, ρ and $\mathbf{u}$ are the density and velocity fields and V is the potential function. Note that there are no explicit solutions for these model equations, and existence steady-state and stability analyses typically cannot be performed. Eulerian models have been studied primarily by simulation quantifying the changes in the model output which come from parameter variation, and categorizing different types of behavior exhibited by the model; we do not present these kinds of results in the thesis. The weakness of such efforts is to lose the clarity afforded by analytical observations, where the relationship between model parameters and group-level properties is made clear.

Chapter 2

A Lagrangian Model of Self-Propelled Particles

2.1 Introduction

Self-organization and pattern formation in systems of self-propelled entities are ubiquitous in nature. Recently the problem of swarming, in which a large number of moving particles (e.g., fish or birds) remain coherent over long times and distances, has attracted considerable attention. Here, we need to accurately predict the geometry and stability of swarming systems and our method is to apply the fundamental principles from statistical mechanics. Specifically, we consider N self-propelled particles powered by biological or mechanical motors that experience a frictional force, leading to a preferred characteristic speed. The particles also interact by means of an interaction potential called Morse potential.

2.2 The Model I

We make the following assumptions [20,37]:

1. The population is conserved; birth, death, immigration, and emigration of organisms are negligible on the time scale of the swarming dynamics.

2. Interactions between organisms are pairwise.

3. Interactions depend only on the distance between organisms and become weaker with increasing distance.

4. The interaction must not cause the collapse of infinitely many particles into a bounded region of $\mathbb{R}^d$.

The discrete particle model we describe here, which satisfies all the conditions in the above, consists of N particles with mass m_i, positions $\mathbf{x}_i$ and velocity $\mathbf{v}_i$. The following equations of motion describe the model [4,5,50]

$$\frac{d\mathbf{x}_i}{dt} = \mathbf{v}_i, \qquad m_i\frac{d\mathbf{v}_i}{dt} = \alpha\mathbf{v}_i - \beta|\mathbf{v}_i|^2\mathbf{v}_i - \nabla U_i, \quad i = 1, 2, ..., N. \tag{2.1}$$

Here U_i is the interaction potential and the terms $\alpha\mathbf{v}_i$ and $-\beta|\mathbf{v}_i|^2\mathbf{v}_i$ are self-acceleration and deceleration which give the particles a tendency to travel close to an equilibrium speed $v_{eq} = \sqrt{\frac{\alpha}{\beta}}$. Note that the self-propelling mechanism allows the direction of motion changes but tends to fix the magnitude of the velocity. In our simulations we have two major solutions which mostly dependent on the initial conditions: circular motion or a coherent agent drift. The potential U_i describes the interaction of particle i with the other particles.

The potential we use here is the Morse potential given as

$$U_i = U(\mathbf{x}_i) = \sum_{j\neq i}(-C_a e^{-\frac{|\mathbf{x}_i-\mathbf{x}_j|}{l_a}} + C_r e^{-\frac{|\mathbf{x}_i-\mathbf{x}_j|}{l_r}}). \tag{2.2}$$

This formula assumes that the N-body interactions are insignificant and only pairwise interactions are considered. We assume $N \geq 3$ not to deal with trivial cases. The pairwise interaction consists of attraction and repulsion with C_a and C_r specifying their respective strengths and l_a, l_r their effective interaction length scales. The potential (2.2) is a combination of other attractive and repulsive terms lead to collective trends and gives interesting aggregation patterns. For simplicity, we only consider a $2D$ description and focus on identical mass particles.

We can non-dimensionalize the equations of motion by substituting $t' = (m_i/l_a^2\beta)t$, $\mathbf{x}_i{}' = \mathbf{x}_i/l_a$, and thus, $\mathbf{v}_i{}' = (l_a\beta/m_i)\mathbf{v}_i$ into equations (2.1) and (2.2)

$$\frac{d\mathbf{x}_i{}'}{dt'} = \mathbf{v}_i{}', \qquad \frac{d\mathbf{v}_i{}'}{dt'} = \alpha'\mathbf{v}_i{}' - |\mathbf{v}_i{}'|^2\mathbf{v}_i{}' - \frac{1}{m_i'}\nabla_{\mathbf{x}_i{}'}U_i' \tag{2.3}$$

$$U_i' = \sum_{j\neq i}(-e^{-|\mathbf{x}_i{}'-\mathbf{x}_j{}'|} + Ce^{-\frac{|\mathbf{x}_i{}'-\mathbf{x}_j{}'|}{l}}) \tag{2.4}$$

where $\alpha' = (\alpha\beta l_a^2)/m_i^2$, $m_i' = m_i^3/(\beta C_a l_a^2)$, $C = C_r/C_a$, and $l = l_r/l_a$; hence, the model is essentially a 4-parameter one.

In our simulations we also use white noise. In this case the particles are subject to stochastic white forces ξ_i of strength D which are independent for different particles and are characterized by the correlation functions

$$\langle\xi_i(t)\rangle = 0, \qquad \langle\xi_i(t)\xi_j(t')\rangle = 2D\delta(t-t')\delta_{ij}$$

Therefore our stochastic differential equation model becomes

$$\frac{d\mathbf{x}_i{}'}{dt'} = \mathbf{v}_i{}', \qquad \frac{d\mathbf{v}_i{}'}{dt'} = \alpha'\mathbf{v}_i{}' - |\mathbf{v}_i{}'|^2\mathbf{v}_i{}' - \frac{1}{m_i'}\nabla_{\mathbf{x}_i{}'}U_i' + \xi_i(t). \tag{2.5}$$

2.3 Stable Interactions

In this section we apply fundamental principles from statistical mechanics to be able to analyze and predict the geometry of swarming systems. Here we follow closely the work of [35]. For N particles located at $\mathbf{x}_1, ..., \mathbf{x}_N \in \mathbb{R}^d$, consider the potential $U(\mathbf{x}_1, ..., \mathbf{x}_N)$ which takes values in $\mathbb{R}\cup\{\infty\}$, i.e., the value ∞ is permitted for the potential energy. We assume that the potential is invariant under permutation of its arguments; because we don't have any preferences in the ordering of our particles and also we follow with its physical meaning (potential energy). Furthermore, we assume that U is invariant under translations: if $\mathbf{a}\in\mathbb{R}^d$, then

$$U(\mathbf{x}_1+\mathbf{a}, ..., \mathbf{x}_N+\mathbf{a}) = U(\mathbf{x}_1, ..., \mathbf{x}_N)$$

If U does not take the value ∞, we may write

$$U(\mathbf{x}_1, ..., \mathbf{x}_N) = \sum_k \sum_{1\leq i_1<...<i_k\leq N} \Phi^k(\mathbf{x}_{i_1}, ..., \mathbf{x}_{i_k}). \tag{2.6}$$

Here we assume that the functions Φ^k are real-valued, invariant under permutations of their arguments and under translations. Equation (2.6) uniquely determines (by induction on k) the k-body potential Φ^k. If U is allowed to take the value ∞, we shall also assume the form (2.6) where Φ^k is now also allowed to take the value ∞. We assume Φ^k to be Lebesgue measurable. Because of translation invariance Φ^1 is a constant; conventionally, we take $\Phi^1 = 0$. Altogether we assume the summation in (2.6) is over $k \geq 2$.

A sequence $(\Phi^k)_{k\geq 2}$ of k-body potentials is called an *interaction*. The 2-body potential Φ^2 is also known as a *pair interaction*. Notice that $\Phi^2(\mathbf{x}_1, \mathbf{x}_2)$ due to translation invariance and therefore it depends only on $\mathbf{x}_1 - \mathbf{x}_2$; we shall write $\Phi^2(\mathbf{x}_1, \mathbf{x}_2) = \Phi(\mathbf{x}_2 - \mathbf{x}_1)$. Now because of invariance under permutation of $\mathbf{x}_1$ and $\mathbf{x}_2$, we have thus $\Phi(-\mathbf{x}) = \Phi(\mathbf{x})$. Finally if a pair potential Φ has compact support then we say Φ is *finite range*.

DEFINITION. *We say that the interaction $(\Phi^k)_{k\geq 2}$ is H-stable if there exists $B \geq 0$ such that*

$$U(\mathbf{x}_1, ..., \mathbf{x}_N) \geq -NB \tag{2.7}$$

for every $N \geq 1$ and $\mathbf{x}_1, ..., \mathbf{x}_N \in \mathbb{R}^d$.

H-stability is actually one of the important constraints which enable us to have a smooth passage from microscopic interactions, obeying the laws of statistical mechanics, to the thermodynamic limit, as volume and individual number tend to infinity. Here we give a useful criteria for the H-stability of pair interactions. Let Λ be a bounded Lebesgue measurable subset of $\mathbb{R}^d$ with volume (=Lebesgue measure) $V(\Lambda)$; define

$$\Xi_\Lambda = 1 + \sum_{n=1}^{\infty} \frac{z^n}{n!} \int_{\Lambda^n} \exp[-\beta U(\mathbf{x}_1, ..., \mathbf{x}_N)] d\mathbf{x}_1 ... d\mathbf{x}_N,$$

with $\beta > 0, z > 0$. H-Stability implies that

$$1+\sum_{n=1}^{\infty}\frac{z^n}{n!}\int_{\Lambda^n}\exp[-\beta U(\mathbf{x}_1,...,\mathbf{x}_N)]d\mathbf{x}_1...d\mathbf{x}_N \leq$$
$$1+\sum_{n=1}^{\infty}\frac{z^n}{n!}V(\Lambda)^n\exp(n\beta B)=\exp[zV(\Lambda)\exp(\beta B)]. \quad (2.8)$$

Therefore the series defining Ξ_Λ is convergent.

Now we need to find a simple criterion to check H-stability; because of this, we consider a class of pair interactions as follows which is pretty large. Let Φ be a real upper semicontinuous function on $\mathbb{R}^d$ such that $\Phi(-\mathbf{x})=\Phi(\mathbf{x})$. Define:

$$U(\mathbf{x}_1,...,\mathbf{x}_N)=\sum_{1\leq i<j\leq N}\Phi(\mathbf{x}_j-\mathbf{x}_i).$$

PROPOSITION. *Let the pair potential Φ be absolutely integrable. If*

$$\int\Phi(\mathbf{x})d\mathbf{x}<0 \quad (2.9)$$

then we may choose Λ bounded such that Ξ_Λ diverges.

Proof. The exponential function is convex thus

$$V(\Lambda)^{-n}\textstyle\int_{\Lambda^n}\exp[-\beta U(\mathbf{x}_1,...,\mathbf{x}_N)]d\mathbf{x}_1...d\mathbf{x}_N \geq \exp[-\beta V(\Lambda)^{-n}\int_{\Lambda^n}U(\mathbf{x}_1,...,\mathbf{x}_N)d\mathbf{x}_1...d\mathbf{x}_N]$$
$$=\exp[-\beta\tfrac{n(n-1)}{2}V(\Lambda)^{-2}\textstyle\int_{\Lambda^2}\Phi(\mathbf{x}_2-\mathbf{x}_1)d\mathbf{x}_1d\mathbf{x}_2].$$

It follows from (2.8) that if we choose for Λ a sufficiently large cube then

$$-\epsilon=V(\Lambda)^{-2}\int_{\Lambda^2}\Phi(\mathbf{x}_2-\mathbf{x}_1)d\mathbf{x}_1d\mathbf{x}_2<0,$$

hence

$$\Xi_\Lambda\geq\sum_{n=1}^{\infty}\frac{z^n}{n!}V(\Lambda)^n\exp[\beta\frac{n(n-1)}{2}\epsilon]=+\infty. \qquad \square$$

If we apply this proposition to the potential given by (2.4) where

$$\Phi(\mathbf{x})=-e^{-|\mathbf{x}|}+Ce^{-\frac{|\mathbf{x}|}{l}},$$

then U is not H-stable if $\int_{\mathbb{R}^d} \Phi(\mathbf{x})d\mathbf{x} \geq 0$. We compute that

$$\begin{aligned}\int_{\mathbb{R}^2} \Phi(x)dx &= \int_0^{2\pi} d\theta \int_0^{\infty} -re^{-r} + Cre^{-r/l}dr \\ &= 2\pi(re^{-r} + e^{-r} - Clre^{-r/l} - Cl^2e^{-r/l})|_0^{\infty} \\ &= 2\pi(Cl^2 - 1).\end{aligned}$$

Therefore the separatrix between stable and non-stable, catastrophic, regions is $Cl^2 = 1$ in the Cl-plane. Note that in Model I we have many coupled ordinary differential equations and if this system obeys the laws of statistical mechanics, thermodynamics is expected to emerge as the number of individuals tend to infinity. In order to get to this limit, H-stability is necessary to the existence of thermodynamics, i.e. if a system is not H-stable, the thermodynamic limit does not exist. The most important property is that H-*stability* ensures that particles will not collapse onto themselves as $N \to \infty$. If the d-dimensional integral of the potential is negative, the system is catastrophic. In this case, as N increases, particles collapse into a dense body with energy per particle proportional to N.

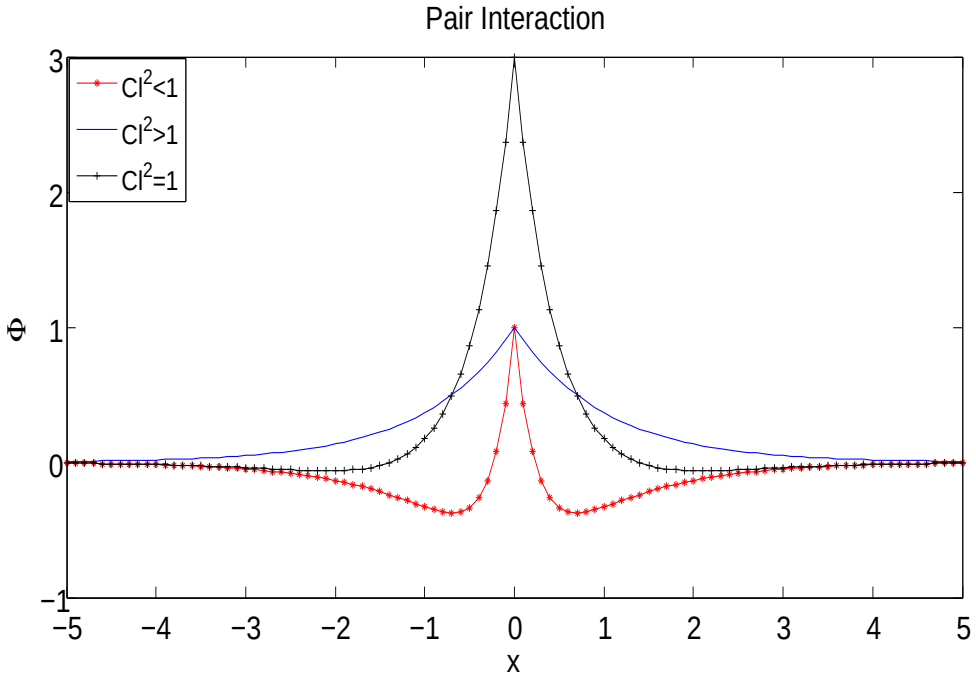

Figure 2.1: Pair interactions, $\Phi(x)$ (in one dimension), for different C and l values.

2.4 Numerical Results

2.4.1 Deterministic Case

In this case we simulate the model by using equations (2.3) and (2.4) where particles are identical, i.e. $m_i = 1$ for all i. With random initial conditions and free boundaries, integration of model I numerically enables us to distinguish different aggregation regimes in the $\{C, l\}$ phase space. In Figure 2.2, we see the biologically relevant region that consist of a long-range attraction and a short-range repulsion corresponding to the parameter space where $C > 1$ and $l < 1$. Three regions I, II and III are distinguished there for $\{l < C\}$, $\{l = C\}$ and $\{l > C\}$. Regions IV, V, VI and VII correspond to the regimes $\{C < 1 < l\}, \min\{l, C\} > 1, \{1/\sqrt{C} < l < 1\}$ and $\{l < 1/\sqrt{C} < 1\}$.

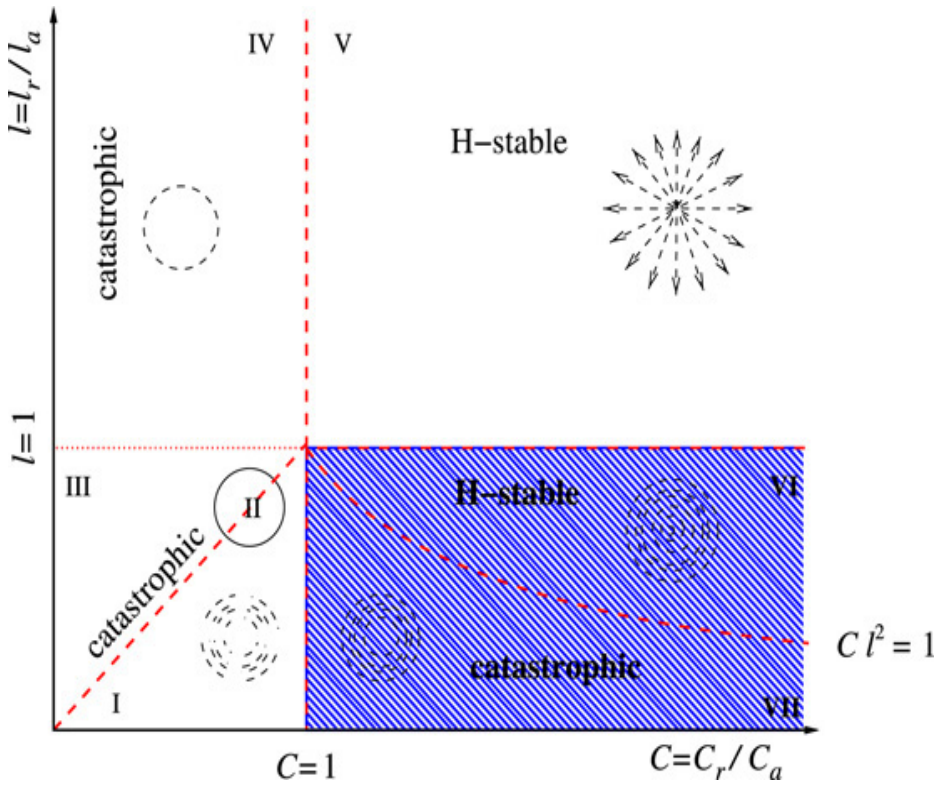

Figure 2.2: H-stability diagram of the Morse potential (taken from [5]). The catastrophic regions correspond to parameter ratios $l = l_r/l_a$ and $C = C_r/C_a$ for which the thermodynamic limit does not exist. The separatrix is $Cl^2 = 1$.

In region I, a potential minimum exists and by creating multiparticle clumps, the N particles self-organize themselves. The individuals have collective translational motions within each clump and rotate about their center of mass. Two examples are shown in Figure 2.3(c) and (d). In region II, the potential minimum is zero and rings develop. For $l > C$ in region III, clumped rings appear although there is no minimum in potential [29]. In this case, the clumps are superimposed particles traveling around a ring. See Figure 2.4(c). In region IV, the observed behaviour is similar to what is described in region III but the potential defines a maximum [30]. In regions III and IV, the collective motion is a way to minimize the total energy while keeping a constant speed [29,30]. For more information about Figure 2.2 see [5,29,30].

Regions I through IV of the phase diagram define catastrophic potentials and structures decrease in size as N increases. In region V the particles will tend to occupy the entire volume at their disposal as $N \to \infty$ [29].

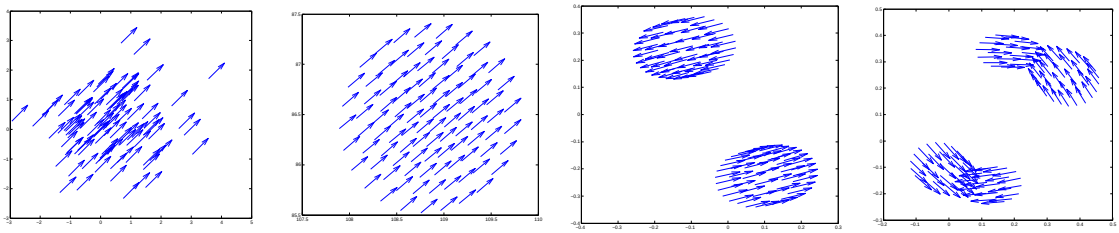

(a) (b) (c) (d)

Figure 2.3: Aggregation geometries for different parameters of equations (2.1) and (2.2) for $N = 100$ individuals at time $t = 100$ except in (d) where time $t = 400$. (a) translational motion (b) a flock (c) rotating clumps (d) rotating double-clumps. In (a) and (b) $C = 2, l = 0.25, \alpha = 1, \beta = 0.5$ and in (c) and (d) $C = 0.6, l = 0.5, \alpha = 1, \beta = 0.5$.

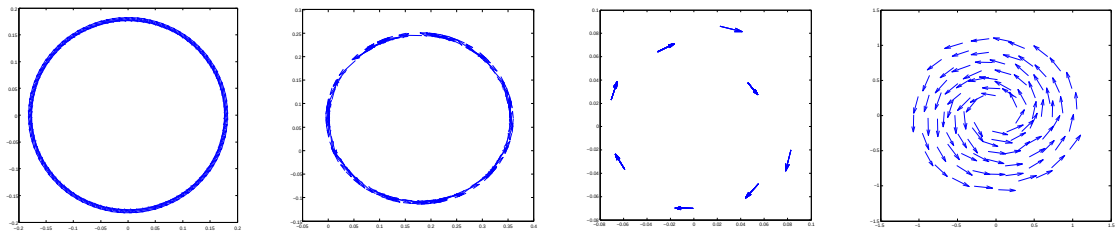

(a) (b) (c) (d)

Figure 2.4: Aggregation geometries for different parameters of equations (2.1) and (2.2) for $N = 100$ individuals at time $t = 100$. (a) ring (b) double-ring (c) ring clump (d) vortex or rotational motion. In (a) and (b) $C = 0.5, l = 0.5, \alpha = 1, \beta = 0.5$ but different initial conditions; in (c) $C = 0.6, l = 1.2, \alpha = 1, \beta = 0.5$ and in (d) $C = 2, l = 0.25, \alpha = 1, \beta = 0.5$.

Regions VI and VII are the most interesting regions in the Figure. For relatively low values of α/β rigid-like motion, like a flock or disk, can form and for the high values of α/β individuals disperse. For region VII, additionally, rotating vortices may be generated for intermediate values of α/β [29]. In Figure 2.3(b), a coherent flock and in Figure 2.4(d) a vortex are shown. Time evolution of a vortex solution with random initial conditions is shown in Figure 2.5.

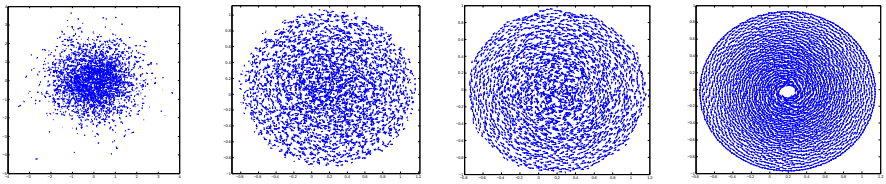

(a) $t = 0$ (b) $t = 10$ (c) $t = 20$ (d) $t = 40$

Figure 2.5: Rotational solution in the catastrophic regime. There are $N = 3000$ individuals and the parameters are $C = 2, l = 0.25, \alpha = 1.6, \beta = 0.5$ at different times.

An interesting phenomenon here is that when we increase the number of individuals,

the diameter of the solutions in the catastrophic region decreases. For example, in Figure 2.4(a), if we plot the radius of the rings versus the number of individuals, we get the Figure 2.6 below, in which the circles are the numerical solution of the radius and the best fit curve is $R(N) = 0.8484N^{-.5669}$ as a function of the number of individuals N. Note that time here is $t = 40$ for each N. We expect that by plotting the radius for larger values of N we will approach the analytical result $N6{-}.5$ obtained in [30]. Similarly if we increase the

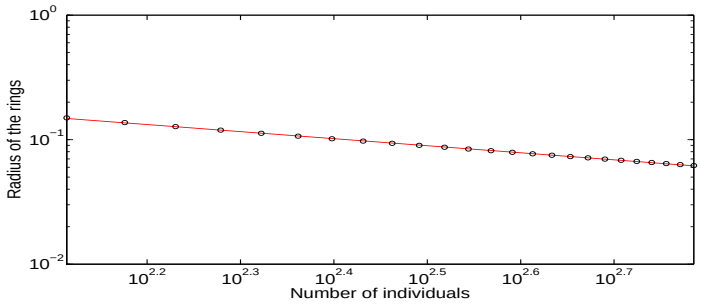

Figure 2.6: Ring size decreases with agent number in the catastrophic regime. The circles are the numeric solution and the curve is the analytic solution. The parameters are the same as in Figure 2.3(a) and time is $t = 40$.

number of individuals in the vortex solution, the diameter and therefore the area decreases. The diameters in (a)-(d) of Figure 2.6 are approximately 2.6336, 2.0321, 1.9289 and 1.9131, respectively.

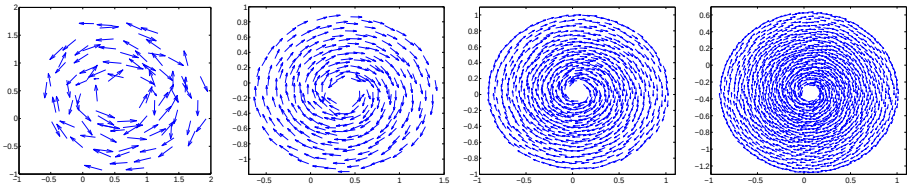

Figure 2.7: Vortex size decreases with agent number in the catastrophic regime. (a)-(d) $N = 100, 300, 800$ and 1500 individuals respectively. The parameters are $C = 2, l = 0.25, \alpha = 1.6, \beta = 0.5$ and time $t = 40$.

In Figure 2.8 the area of the vortex solutions versus the number of individuals is

illustrated. The circles are from the numerical solution and the analytical solution is $A(N) = 5.033\exp(-.0111N) + 2.8518$ as a function of the number of individuals N.

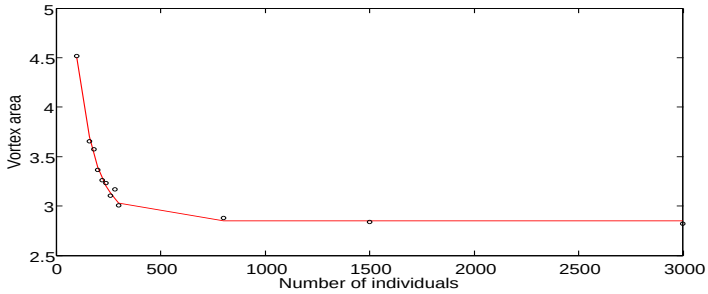

Figure 2.8: Vortex area decreases with agent number in the catastrophic regime. The circles are from the numerical solution and the curve is the analytic solution. The parameters are the same as in Figure 2.6 and time is $t = 40$.

We may also find the inner radius and the outer radius of the vortex solution for different number of individuals. In Figure 2.9, the numerical solution for the outer radius is represented by circles and the analytical solution is $OR(N) = .8516\exp(-.0111N) + .9565$.

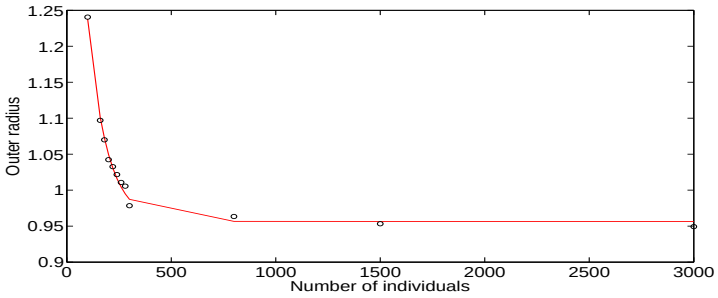

Figure 2.9: Outer radius decreases with agent number in the catastrophic regime. The circles are from the numerical solution and the curve is the analytic solution. The parameters are the same as in Figure 2.6 and time is $t = 40$.

To find the inner radius $IR(N)$, as a function of the number of individuals N, we can write

$$IR(N) = \sqrt{(\pi OR(N)^2 - A(N))/\pi}$$

2.4.2 Noise-induced Case

One of the most interesting aspects of many particle systems is that they exhibit a complex cooperative behaviour during phase transition. When we increase the noise strength transitions could happen. For example, below we see the transition from a translational solution to a rotational solution. The following graph shows the transition with the above

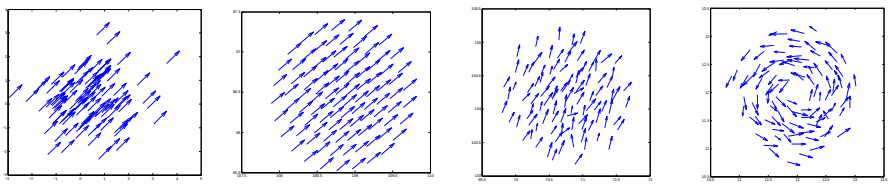

(a) initial data (b) $D = 0$ (c) $D = 0.06$ (d) $D = 0.07$

Figure 2.10: Noise induced phase transition for $N = 100$ individuals. (a) initial configuration with random positions and fixed velocity. (b)-(d) solution at time= 100 corresponding to $D = 0, 0.06$ and 0.07, respectively. The other parameters are $C = 2, l = 0.25, \alpha = 1, \beta = 0.5$.

parameters. The translational motion breaks down when a critical intensity is reached and instead the swarm goes into a rotational mode.

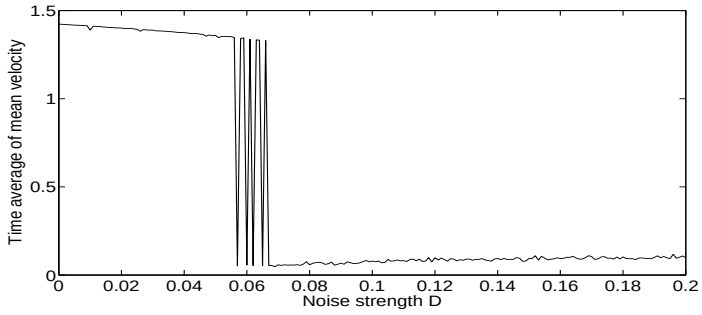

Figure 2.11: Time average of Euclidean norm of mean velocity, $\mathbf{V}(t) = (1/N)\sum_i \mathbf{v}_i(t)$, versus noise strength, upto time $t = 300$.

As we see, there are some bumps in the transition diagram, Figure 2.11. At the bottom of each bump the solution is rotational, as in Figure 2.10(d), and at the top the solution is semi-translational, as in Figure 2.10(c). Figure 2.11 is different from the similar one in [15], where there is exactly one sharp jump rather than several fluctuations. Note the state transition from a translational state, $|V| \simeq 1.3$ to a rotational state, $|V| \simeq 0.01$ that occurs at the interval $[0.04, 0.09]$. Our numerical experiments with various different realizations of the noise, taking time averages over times up to 600, have not shown a systematic reduction of the parameter interval in D over which the transition occurs; and further ensemble averaging appears to smear out the transition. In our computations we have not observed a single sharp transition, as seen in [15] but the results are preliminary and inconclusive. The following figure shows the evolution of the size of mean velocity in time for different noise strengths. In Figure 2.12, as we expect from Figure 2.11, the mean velocity suddenly decreases for the D values corresponding to the rotational solutions. These figures are for single realization.

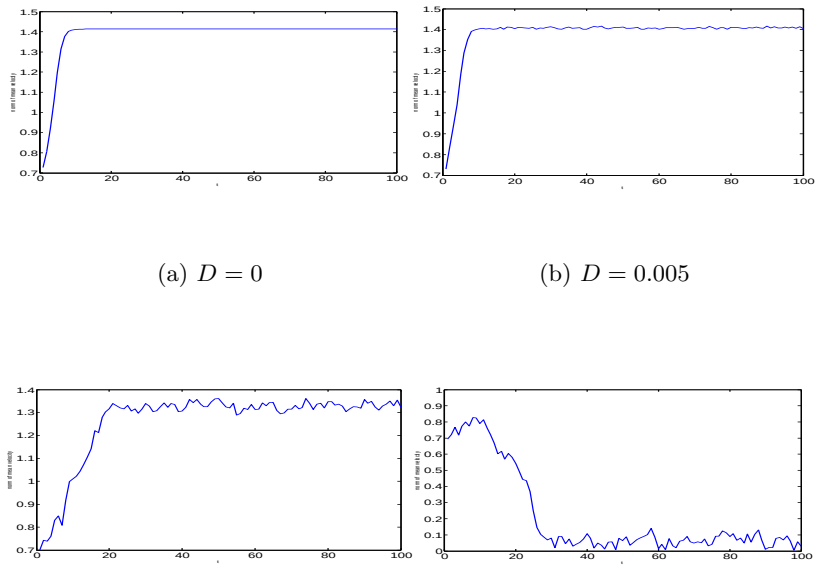

(a) $D = 0$ (b) $D = 0.005$

(c) $D = 0.06$ (d) $D = 0.07$

Figure 2.12: norm of mean velocity, $\mathbf{V} = (1/N) \sum_i \mathbf{v}_i(t)$, versus time for different values of the noise strength D.

Chapter 3

A Stochastic Model of Interacting Particles

3.1 Introduction

In this chapter we consider a model of a population of self-propelled particles interacts via a parabolic interaction potential corresponding to linear attracting forces between the pairs [14,23]. In the absence of noise, this dynamical system has two kinds of attractors, corresponding, respectively, to a compact traveling state of the entire population and to a state where it rotates as a vortex without any global translational motion [14]. We see that the system is highly sensitive to stochastic forces. When noise is present, the traveling swarm is a cloud of particles characterized by different dispersions in the directions parallel and transverse to the direction of translational motion. When the noise is increased, the swarm gradually acquires a more symmetric shape. For strong noise, we find that the translational motion of the swarm is replaced by a rotational regime with a vortex flow. We also present an extension of this model in which we use random attraction coefficients. We find new solutions and a transition behaviour and consider Voronoi diagrams.

3.2 Model II

In this chapter we mostly are interested in rotational motions that are excited by negative velocity-dependent linear friction terms and interaction forces that can be described by a mean field. In the book of Okubo and Levin [28], it is discussed that animal groups have three typical modes of motion: (i) translational motion, (ii) rotations or (iii) amoeba-like motions.

The simple and interesting model we consider here composed of active Brownian particles. Active Brownian particles are Brownian particles with the ability to take up energy from the environment and use it for acceleration [14]. Therefore, in our case, the self-propulsion is modeled by active Brownian particles with negative friction which are capable of converting stored internal energy into motion.

We consider a swarm formed by N point masses m with the numbers $1, 2, ..., N$ via linear pair interactions $\omega^2(\mathbf{r}_i - \mathbf{r}_j)$. The coefficient ω^2 identifies the intensity of interactions and also as a parameter can specify the strength of coupling in population [10,23]. The dynamics of the system is given by the following equations of motions:

$$\dot{\mathbf{r}}_i = \mathbf{v}_i, \qquad m\dot{\mathbf{v}}_i = F_i(\mathbf{v}_i) - \omega^2(\mathbf{r}_i - \mathbf{R}(t)) + \sigma^2(\mathbf{v}_i - \mathbf{V}) + \xi_i(t), \tag{3.1}$$

where the center of mass is defined by $\mathbf{R}(t) = \frac{1}{N}\sum_{j=1}^{N}\mathbf{r}_j$ and the dissipative forces are

$$F_i(\mathbf{v}_i) = -m\gamma(\mathbf{v}_i^2)\mathbf{v}_i.$$

The function γ denotes a velocity-dependent friction, and we use the traditional Ansatz proposed already by Rayleigh [33]:

$$\gamma(\mathbf{v}^2) = -(\alpha - \beta|\mathbf{v}|^2).$$

We see that the zero of the friction $\gamma(\mathbf{v}^2) = 0$ exists which in the velocity space is an attractor of motion. The term $\mathbf{V}$ models a weak global coupling to the average velocity of the swarm $\mathbf{V} = \frac{1}{M}\sum m_i\mathbf{v}_i$. We also make another assumption that the global coupling of the velocities will be neglected, $\sigma = 0$.

As in the previous section, the particles are subject to stochastic white noise forces ξ_i of strength D which are independent for different particles and are characterized by the correlation functions, first and second moments:

$$\langle \xi_i(t) \rangle = 0, \qquad \langle \xi_i(t)\xi_j(t') \rangle = 2D\delta_{ij}\delta(t-t'),$$

where the average $\langle \cdot \rangle$ is an average with respect to the distribution of the realization of the stochastic variable $\xi(t)$.

3.3 The Weak Noise Limit

Here we will restrict our attention to the case of weak driving forces and follow the work of Erdmann *et al* [15]. Due to the anisotropic motion of a swarm in the presence of noise, we need to somehow measure their dispersions to the direction of its instantaneous mean velocity $\mathbf{V}$. We define parallel dispersion ($S_{||}$) and orthogonal dispersion ($S_{\perp}$) as

$$S_{||}(t) = \frac{1}{NV^2(t)} \sum_{i=1}^{N} \{[\mathbf{r}_i(t) - \mathbf{R}(t)] \cdot \mathbf{V}(t)\}^2$$

$$S_{\perp}(t) = \frac{1}{NV^2(t)} \sum_{i=1}^{N} \{[\mathbf{r}_i(t) - \mathbf{R}(t)] \times \mathbf{V}(t)\}^2,$$

where $V = |\mathbf{V}|$. In this section when the noise intensity is small, $D \to 0$, we find some analytical expressions for $S_{||}$ and $S_{\perp}$.

By using the fact that the motion of the center of mass will remain approximately linear [15], we consider the coordinate system in such a way that its x axis is parallel to the direction of the swarm motion and its y axis is orthogonal to it. For particle i, write

$$x_i = X + \delta x_i, \qquad y_i = Y + \delta y_i$$

where (X, Y) are the coordinates of the center of mass $\mathbf{R}$. By construction we assume that $Y = 0$. We notice that

$$X(t) = \frac{1}{N} \sum_{i=1}^{N} x_i(t) = \langle x_i(t) \rangle;$$

therefore the equations of motion are

$$\ddot{X} + \delta\ddot{x}_j = \alpha(\dot{X} + \delta\dot{x}_j) - \beta((\dot{X} + \delta\dot{x}_j)^2 + \delta\dot{y}_j{}^2)(\dot{X} + \delta\dot{x}_j) - \omega^2\delta x_j + \xi_j^x(t),$$
$$\delta\ddot{y}_j = \alpha\delta\dot{y}_j - \beta((\dot{X} + \delta\dot{x}_j)^2 + \delta\dot{y}_j{}^2)(\delta\dot{y}_j) - \omega^2\delta y_j + \xi_j^y(t).$$

By neglecting the higher order terms in the first equation, we get

$$\begin{aligned}\ddot{X} + \ddot{\delta x_j} &= \alpha(\dot{X} + \dot{\delta x_j}) - \beta(\dot{X}^3 + 2\dot{X}^2\dot{\delta x_j} + 3\dot{X}\dot{\delta x_j}^2 + \dot{\delta y_j}^2\dot{X}) - \omega^2\delta x_j + \xi_j^x(t), \qquad (3.2)\\ \ddot{\delta y_j} &= \alpha\dot{\delta y_j} - \beta(\dot{X}^2\dot{\delta y_j} + 2\dot{X}\dot{\delta x_j}\dot{\delta y_j} + \dot{\delta y_j}^3) - \omega^2\delta y_j + \xi_j^y(t),\end{aligned}$$

and now if we take the average of equation (3.2) over all indices j, we have

$$\ddot{X} = (\alpha - \beta\dot{X}^2)\dot{X} - 3\beta\dot{X}\langle\dot{\delta x_j}^2\rangle - \beta\dot{X}\langle\dot{\delta y_j}^2\rangle, \qquad (3.3)$$

$$\ddot{\delta y_j} = (\alpha - \beta\dot{X}^2)\dot{\delta y_j} - 2\beta\dot{X}\dot{\delta x_j}\dot{\delta y_j} - \beta\dot{\delta y_j}^3 - \omega^2\delta y_j + \xi_j^y(t). \qquad (3.4)$$

Note that when a swarm travels then $\dot{X} = V \neq 0$ and in the steady state $\dot{X} = V = const$; from equation (3.3) we compute that

$$V^2 = \frac{\alpha}{\beta} - 3\langle\dot{\delta x_j}^2\rangle - \langle\dot{\delta y_j}^2\rangle. \qquad (3.5)$$

Now by subtracting equation (3.3) from equation (3.2) we get the evolution equation for δx_j,

$$\ddot{\delta x_j} = \alpha\dot{\delta x_j} - 2\beta\dot{X}^2\dot{\delta x_j} - \omega^2\delta x_j + \xi_j^x(t),$$

so we see that the fluctuations of $x_j(t)$ are not coupled to the δy_j's . Similarly, in equation (3.4), if we neglect the higher order terms, we would have,

$$\ddot{\delta y_j} - (\alpha - \beta\dot{X}^2)\dot{\delta y_j} + \omega^2\delta y_j = \xi_j^y(t).$$

According to [15] we cannot neglect the higher order terms in the above equation and $\langle\dot{\delta y_j}^2\rangle \gg \langle\dot{\delta x_j}^2\rangle$ holds in the weak noise limit. Hence, from equation (3.5) we may write $V^2 = \frac{\alpha}{\beta} - \langle\dot{\delta y_j}^2\rangle$ and equation (3.4) becomes

$$\ddot{\delta y_j} - \beta(\langle\dot{\delta y_j}^2\rangle - \dot{\delta y_j}^2)\dot{\delta y_j} + \omega^2\delta y_j = \xi_j^y(t),$$

and we see that this SDE does not include longitudinal fluctuations δx_j. In the above equation the particles are decoupled; therefore by dropping the indices we get

$$\ddot{\delta y} - \beta(\langle\dot{\delta y}^2\rangle - \dot{\delta y}^2)\dot{\delta y} + \omega^2\delta y = \xi(t) \qquad (3.6)$$

where $\langle\xi(t)\xi(t')\rangle = 2D\delta(t - t')$.

Now we introduce the slowly varying amplitudes

$$\delta y(t) = \eta(t)e^{i\omega t} + \eta^*(t)e^{-i\omega t},$$

where $\eta(t) = \mu(\epsilon t)$, ϵ is a small constant and to derive a solution we assume that $\omega \gg 1$. By starting from

$$\delta y = \mu(\epsilon t)e^{i\omega t} + \mu^*(\epsilon t)e^{-i\omega t},$$

and taking the derivative of this equation, we get

$$\dot{\delta y} = \epsilon\dot{\mu}(\epsilon t)e^{i\omega t} + i\omega\mu(\epsilon t)e^{i\omega t} + \epsilon\dot{\mu^*}(\epsilon t)e^{-i\omega t} - i\omega\mu^*(\epsilon t)e^{-i\omega t}.$$

In the following steps, we retain those terms that eventually appear in the coefficient of $e^{i\omega t}$. Ignoring the terms with higher powers of ϵ we get

$$\dot{\delta y}^2 \sim 2i\omega\epsilon\mu\mu^* - 4i\omega\epsilon\dot{\mu}\mu^* + 2\omega^2\mu\mu^* \sim 2\omega^2|\mu|^2,$$

and similarly

$$\dot{\delta y}^3 \sim (i\omega\mu e^{i\omega t} - i\omega\mu^* e^{-i\omega t})^3 \sim 3i\omega^3\mu|\mu|^2 e^{i\omega t};$$

also, taking ensemble averages implies that

$$\dot{\delta y}\langle\dot{\delta y}^2\rangle \sim 2i\omega^3\langle|\mu|^2\rangle\mu e^{i\omega t}.$$

We also similarly take the second derivative

$$\ddot{\delta y} \sim \frac{d}{dt}(\epsilon\dot{\mu}(\epsilon t)e^{i\omega t} + i\omega\mu e^{i\omega t}) \sim 2i\omega\epsilon\dot{\mu}(\epsilon t)e^{i\omega t} - \omega^2\mu e^{i\omega t}.$$

Therefore we can rewrite equation (3.6) as

$$2i\omega\epsilon\dot{\mu}(\epsilon t)e^{i\omega t} - 2i\beta\omega^3\langle|\mu|^2\rangle\mu e^{i\omega t} + 3i\omega^3\mu|\mu|^2 e^{i\omega t} = \xi(t)$$

or

$$\dot{\eta} = \beta\omega^2\eta\langle|\eta|^2\rangle - \frac{3}{2}\omega^2\eta|\eta|^2 + \zeta(t),$$

where the complex-valued white noise $\zeta(t)$ has correlation functions

$$\langle\zeta(t)\rangle = 0, \qquad \langle\zeta(t)\zeta(t')\rangle = 0, \qquad \langle\zeta(t)\zeta^*(t')\rangle = \frac{D}{2\omega^2}\delta(t-t').$$

Now to be able to use the numerical data in [15], we assume that $\alpha = \beta = 1$. To derive the Fokker-Planck equation for this stochastic Langevin equation with the probability density $P = P(\eta, \eta^*, t)$, we note that for the SDE

$$\frac{dX}{dt} = \bigtriangledown\psi(X(t)) + \sqrt{\frac{2}{B}}\zeta(t),$$

the corresponding Fokker-Planck equation is

$$\frac{\partial P}{\partial t} = -\mathrm{div}(\bigtriangledown\psi(X)P) + \frac{1}{B} \bigtriangleup P,$$

and the stationary solution is

$$\bar{P}_s(x) = z^{-1} \exp(-B\psi(x)),$$

where $z = \int_{\Re^N} \exp(-B\psi(x))dx$ [16]. In our case, we have $X = (\eta, \eta^*)$ and

$$\psi(X) = \omega^2\langle|\eta|^2\rangle|\eta|^2 - \frac{3}{4}\omega^2|\eta|^4,$$

therefore,

$$\begin{aligned}\frac{\partial P}{\partial t} = &-\frac{\partial}{\partial\eta}[\omega^2(\langle|\eta|^2\rangle\eta - \frac{3}{2}|\eta|^2)\eta P] \\ &- \frac{\partial}{\partial\eta^*}[\omega^2(\langle|\eta|^2\rangle\eta - \frac{3}{2}|\eta|^2)\eta^* P] \\ &+ \frac{D}{2\omega^2}\frac{\partial^2 P}{\partial\eta\partial\eta^*}.\end{aligned}$$

The stationary solution of the Fokker-Planck equation is

$$\bar{P} = \frac{1}{Z}\exp[\frac{-\omega^4}{D}(-4\langle|\eta|^2\rangle|\eta|^2 + 3|\eta|^4)]$$

where

$$Z = \int_{\Re^N} \exp[\frac{-\omega^4}{D}(-4\langle|\eta|^2\rangle|\eta|^2 + 3|\eta|^4)]d^2\eta;$$

note that here, $d^2\eta = d\eta_1 d\eta_2$ for $\eta = (\eta_1, \eta_2)$. Now the second statistical moment is given by

$$\langle|\eta|^2\rangle = \int |\eta|^2 \bar{P}(\eta, \eta^*)d^2\eta. \tag{3.7}$$

Let $\eta = \rho e^{i\phi}$, then $d^2\eta = \rho d\rho d\phi$, and we can rewrite equation (3.7) as

$$\langle\rho^2\rangle = \frac{\int_0^\infty \rho^3 \exp[\frac{-\omega^4}{D}(-4\langle\rho^2\rangle\rho^2 + 3\rho^4)]d\rho}{\int_0^\infty \rho \exp[\frac{-\omega^4}{D}(-4\langle\rho^2\rangle\rho^2 + 3\rho^4)]d\rho}.$$

By taking $u = \rho\langle|\eta|^2\rangle^{-1/2}$, this equation becomes

$$1 = \frac{\int_0^\infty u^3 \exp[-\nu(-4u^2 + 3u^4)]du}{\int_0^\infty u \exp[-\nu(-4u^2 + 3u^4)]du} \tag{3.8}$$

where $\nu = \frac{\omega^4}{D}\langle|\eta|^2\rangle^2$ and $\nu \approx 0.22$ [15]. Therefore

$$\langle|\eta|^2\rangle = \nu^{1/2} D^{1/2} \omega^{-2}.$$

It can be easily shown that $S_\perp = \langle \delta y^2 \rangle = 2\langle|\eta|^2\rangle$ and $S_{||} = \langle \delta x^2 \rangle$. Hence,

$$S_\perp = \kappa \frac{D^{1/2}}{\omega^2},$$

where $\kappa = 2\nu^{1/2} \approx 0.94$, and

$$S_{||} = \frac{D}{2\omega^2}$$

We see that in the limit $D \to 0$ the transversal dispersion depends on $\sqrt{D}$ but the parallel dispersion depends linearly on D. Therefore when D is small number, $S_\perp$ is much larger than $S_{||}$. When the noise strength D increases, the shape of the motion becomes more symmetric and it changes from translational solution to rotational solution. In this case, the transversal dispersion approaches the dispersion along the direction of translational motion.

3.4 The Extended Model II

We consider a swarm formed by N identical self-propelled particles of unit mass interacting via an attractive parabolic pair potential. The dynamics of the system is given by the following set of evolution equations:

$$\dot{\mathbf{r}}_i = \mathbf{v}_i, \qquad \dot{\mathbf{v}}_i = \alpha \mathbf{v}_i - \beta |\mathbf{v}_i|^2 \mathbf{v}_i - \frac{a_i}{N} \sum_{j=1}^{N} (\mathbf{r}_i - \mathbf{r}_j) + \xi_i(t), \tag{3.9}$$

for $i = 1, 2, ..., N$, where α and β are constants, a_i's are random and $\xi_i(t)$'s are stochastic white forces of strength D which are independent for different particles and are characterized by the correlation functions

$$\langle \xi_i(t) \rangle = 0, \qquad \langle \xi_i(t) \xi_j(t') \rangle = 2D\delta_{ij}\delta(t - t').$$

The only difference this model has with the model II is the attraction coefficients a_i which are different for individuals. We generate these coefficients such that are normally distributed. In all the figures below, we have 100 individuals; 10 are black with $\{a_i\}_1^{10} \sim 500 + \mathcal{N}(0, 1)$, 10 are red with $\{a_i\}_{11}^{20} \sim 100 + \mathcal{N}(0, 1)$ and the rest are green with

$\{a_i\}_{21}^{100} \sim 3 + \mathcal{N}(0,1)$. By this choice of the values of a_i we are going to illustrate that the magnitude of a_i is an important scale that the diameter of the solutions of this model depend on. Here we have three different magnitudes for a_i which are 500, 100 and 3.

There are some new solutions that this model gives us. In Figure 3.1, we have a semi-translational motion. Individuals of the same colour group together and each group has a coherent motion which is almost translational. Another interesting solution is the triple double-mill shown in Figure 3.2(b). Individuals of the same colour (same magnitude of a_i) group together and have a double mill motion as we may have for the model II (a double-mill solution is a vortex with some particles moving clockwise and the rest moving counter clockwise). Note that because we start with three different magnitudes for a_i, we end up with three double-mills. If we start with for example 10 different magnitudes, we get 10 double-mill solutions.

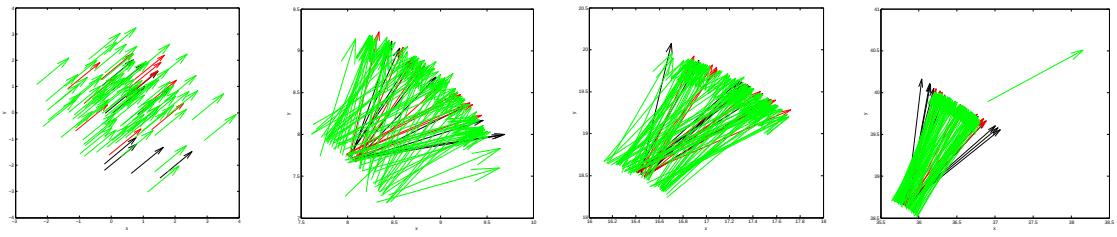

(a) time= 0 (b) time= 10 (c) time= 20 (d) time= 40

Figure 3.1: Semi-translational solution. $N = 100$ individuals with random initial positions and constant velocity, shown in (a), evolving according to the equation (3.9). There are 10 black and 10 red individuals and the rest are all coloured green. The parameters are $\alpha = 2, \beta = 1$. a_i is approximately $500, 100$ and 3 for the black, red and green arrows, normally distributed, respectively. Here, the noise strength is $D = 0$.

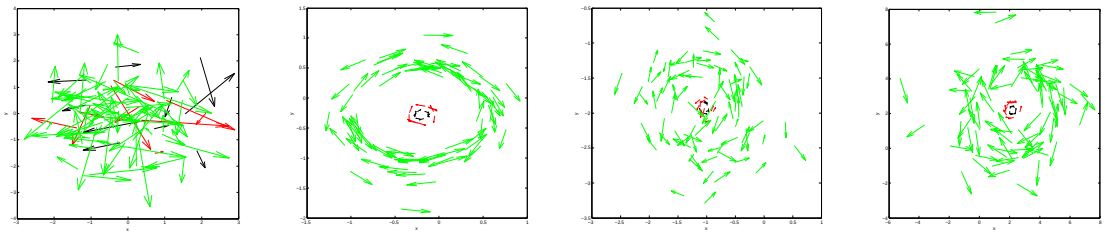

(a) initial condition (b) $D = 0$ (c) $D = 0.15$ (d) $D = 0.4$

Figure 3.2: Triple double-mill solutions. $N = 100$ individuals with random initial conditions, shown in (a), evolving according to the equation (3.9). There are 10 black and 10 red individuals and the rest are all coloured green. Time= 100 and the other parameters are $\alpha = 2, \beta = 1$ but in (d) $\alpha = 20$. a_i is approximately $500, 100$ and 3 for the black, red and green arrows, normally distributed, respectively.

In all the figures in this section, the individuals with higher value of a_i have a higher velocity. The lengths of arrows indicating velocities in the triple double-mill solutions have been rescaled for illustration purposes. This model is more robust compared to model II in the sense of not changing the type of motion by increasing the noise strength. In Figure 3.2, we see that when the noise is $D = 0.15$ we still have triple-double-mill solutions whereas we could not have this for model II. We also note that if we increase the value of α, we need a much larger noise strength, $D = 0.4$ than before to break down the solution.

As we see in Figure 3.3 and 3.4, by increasing the noise strength, the motion changes type from semi-translational to triple double-mill solutions. We obtained a bifurcation diagram similar to the one presented in Figure 2.7 obtained for model I. In addition, numerical experiments suggest that model II may experience a different type of state transition, where by increasing the noise strength, the motion changes first from semi-translation to triple double-mill, then changes back to semi-translation, and finally returns and remains in the triple double-mill state.

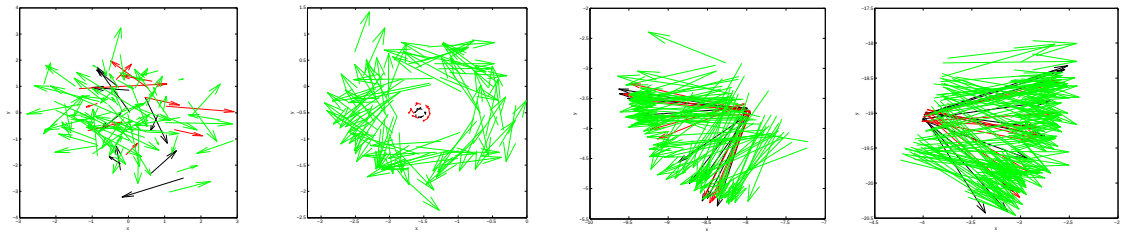

(a) time= 0 (b) time= 10 (c) time= 20 (d) time= 40

Figure 3.3: $N = 100$ individuals with random initial conditions, shown in (a), evolving according to the equation (3.9). There are 10 black and 10 red individuals and the rest are all coloured green. The parameters are $\alpha = 2, \beta = 1$ in (b)-(d). Here a_i are approximately $500, 100$ and 3 for the black, red and green arrows, normally distributed, respectively, and the noise strength is $D = 0.01$

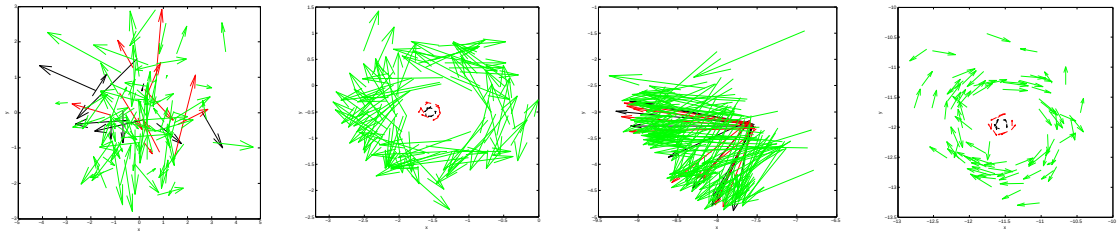

(a) time= 0 (b) time= 10 (c) time= 20 (d) time= 40

Figure 3.4: $N = 100$ individuals with random initial conditions, shown in (a), evolving according to the equation (3.9). There are 10 black and 10 red individuals and the rest are all coloured green. The parameters are $\alpha = 2, \beta = 1$ in (b)-(d). Here a_i are approximately $500, 100$ and 3 for the black, red and green arrows, normally distributed, respectively, and the noise strength is $D = 0.02$

In Figure 3.5 the radius in the double-mill solution versus the attraction coefficients is shown for numerical simulations with a common fixed value of a_i for all i and for $N = 200$; figures for other N look similar. The circles are from the numerical solutions and the best fit curve is $R(a, N) = C_2(N)a^{C_1(N)}$ as a function of the attraction coefficient a and the number of individuals N, where $C_1(N) = 1.6962 \times 10^{-8}N - 4.8438 \times 10^{-1}$ and $C_2(N) = 1.6159 \times 10^{-6}N + 1.3774$, for N varying between 50 and 600, and for a ranging from 1 to 680.

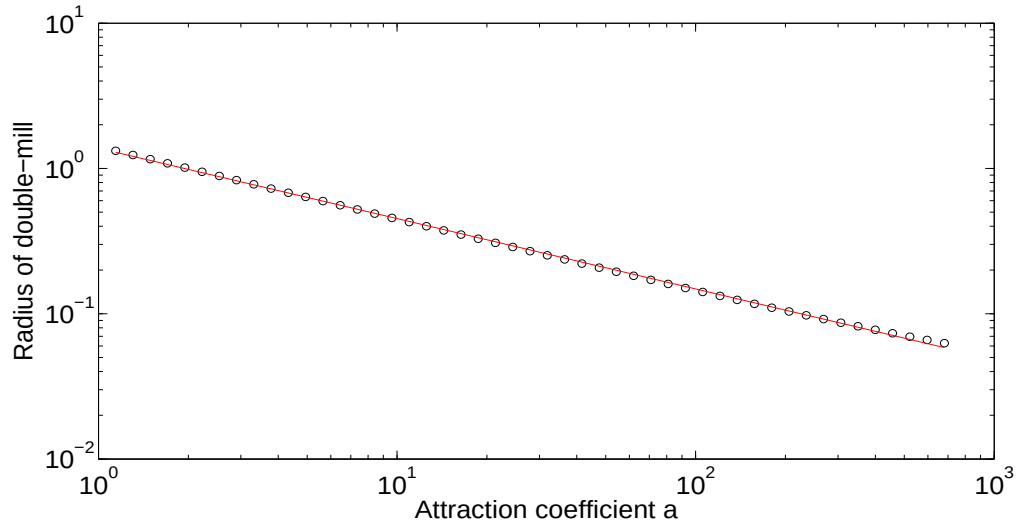

Figure 3.5: The radius in the double-mill solution versus a for constant attraction coefficients a and $N = 200$.

Figure 3.6 shows a similar calculation, in the case in which the values a_i are randomly distributed about a common mean a, with a distribution $a_i \sim a(1 + 0.1\mathcal{N}(0, 1))$. In this case, we fit the radius with $R(a, N) = C_2(N)a^{C_1(N)}$ where $C_1(N) = -3.4987 \times 10^{-6}N - 4.8623 \times 10^{-1}$ and $C_2(N) = 1.5033 \times 10^{-4}N + 1.5048$, and observe the good agreement with the deterministic case shown in Figure 3.5.

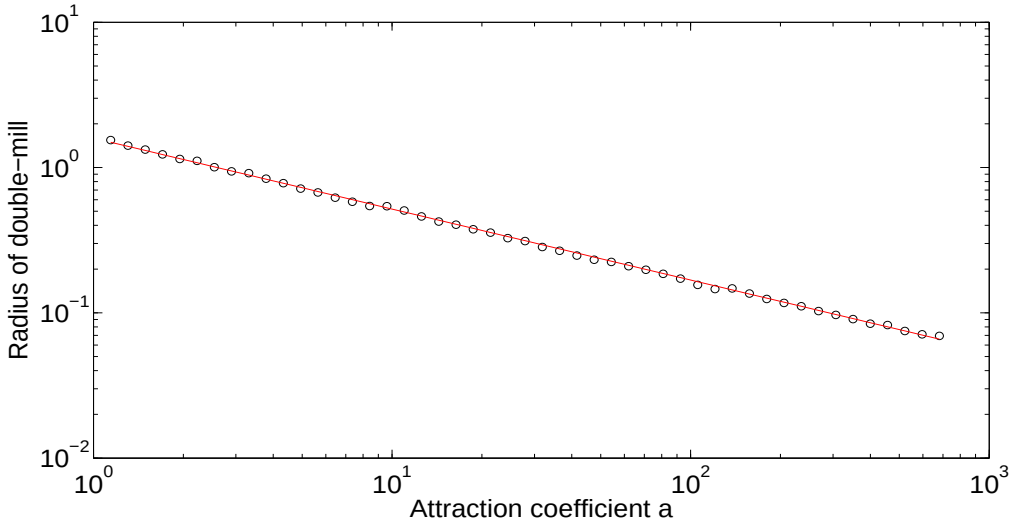

Figure 3.6: The radius in the double-mill solution versus a for random attraction coefficients a and $N = 200$.

Voronoi Diagram Now consider a triple-double-mill solution and its Voronoi diagram for the green individuals (see Figure 3.5(a)). Each individual i has a Voronoi cell consisting of all points closer to i than to any other individual. We have drawn these Voronoi cells in Figure 3.5(a). Now consider the bounded regions and compute their areas. For any noise strength, find the median of the areas of these cells. We find out that the median is increasing by increasing the noise strength and it is almost constant in time for a fixed noise strength. In biology, see for example [39], each cell is called a "domain of danger" and a hidden predator will attack the nearest animal. Figure 3.5(b) might say that if some predators attack a group of animals, in some situations, each prey in the group will distance itself from the others although we can consider them still as a swarm. Therefore, for some animals which follow the extended model II, they follow this strategy of moving away from each other when a predator attacks.

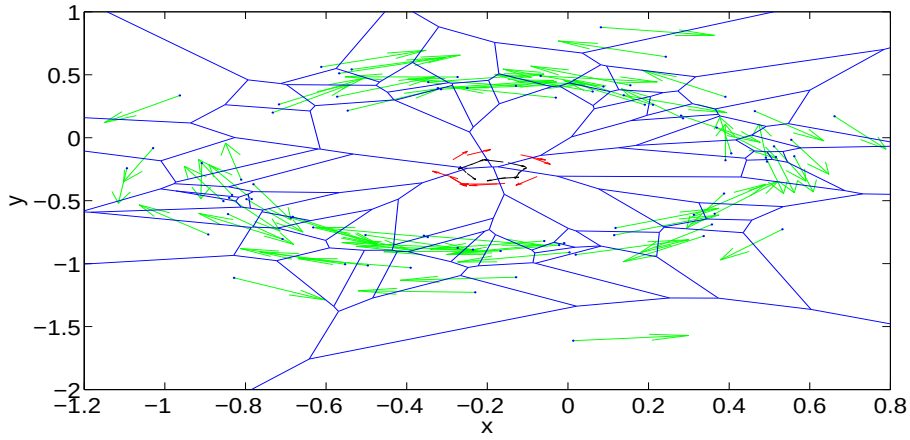

(a)

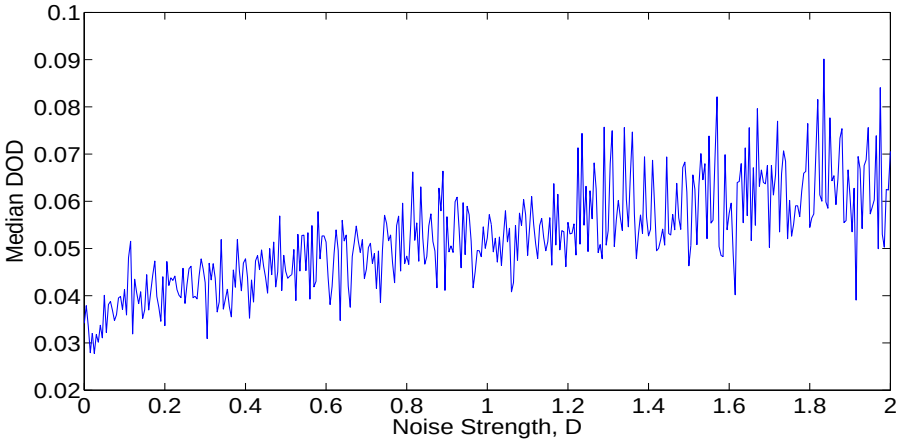

(b)

Figure 3.7: Voronoi diagram for $N = 100$ individuals. There are 10 black and 10 red individuals and the rest are all coloured green. The parameters are $\alpha = 1.5, \beta = 1$ and time= 100. Here a_i are approximately $500, 100$ and 3 for the black, red and green arrows, normally distributed, respectively. (a) The Voronoi diagram for the green individuals, (b) the increase of the median of area of Voronoi cells by increasing noise strength.

Chapter 4

Continuum limits

4.1 Introduction

When we consider massive movements of populations on the ecological scales, the continuum approach is widely adopted for modeling swarming systems which is easy and more suitable for theoretical analysis especially when N goes to infinity.

As we know there is a gap between the individual rules and continuum fluxes and most continuum models in the literature are constructed on the basis of heuristic arguments. To attempt to find a connection, here we derive a continuum model by explicitly calculating the ensemble average of the models I and II by using a probability distribution function. By starting from a microscopic collection of N particles, we derive the continuum hydrodynamic equations.

Before getting to the statistical mechanical theory, we briefly derive fluid dynamics equations, i.e. the continuity equation, the hydrodynamical equation of motion and the energy transport equation. The presentation follows very closely the work of [18]. Consider a continuous fluid consisting of a single chemical component with mass density $\rho(\mathbf{x};t)$ and local velocity $\mathbf{u}(\mathbf{x};t)$ at the point $\mathbf{x}$ and at the time t. Somewhere in the interior of the fluid, take ω as a fixed region. As we know, the mass of the fluid within ω is given by $\int_\omega \rho(\mathbf{x};t)d\omega$. The influx of fluid through the boundary causes the increase of mass

$$\int_\omega \frac{\partial}{\partial t}\rho d\omega = -\int_S \rho\mathbf{u}\cdot d\mathbf{S} = -\int_\omega \nabla_{\mathbf{x}}\cdot[\rho\mathbf{u}]d\omega,$$

where S is the boundary of ω and the surface integral has been converted to a volume integral by Gauss' theorem. Finally, since ω is arbitrary, we get the continuity equation by equating the integrals

$$\frac{\partial}{\partial t}\rho(\mathbf{x};t) = -\nabla_{\mathbf{x}} \cdot [\rho(\mathbf{x};t)\mathbf{u}(\mathbf{x};t)]. \tag{4.1}$$

To derive the hydrodynamical equation of motion, we should equate the the rate of change of momentum within ω, plus the rate of flow of momentum out through the surface of ω, to the sum of the forces acting on the fluid within ω. These forces are the body force and the surface force. Therefore we have

$$\int_\omega \frac{\partial}{\partial t}[\rho(\mathbf{x};t)\mathbf{u}(\mathbf{x};t)]d\omega + \int_S \rho(\mathbf{x};t)\mathbf{u}(\mathbf{x};t)\mathbf{u}(\mathbf{x};t)\cdot d\mathbf{S} = \int_\omega \mathbf{X}(\mathbf{x};t)d\omega + \int_S \sigma(\mathbf{x};t)\cdot d\mathbf{S},$$

or

$$\int_\omega \frac{\partial}{\partial t}[\rho(\mathbf{x};t)\mathbf{u}(\mathbf{x};t)]d\omega + \int_\omega \nabla_{\mathbf{x}} \cdot [\rho\mathbf{u}\mathbf{u}]d\omega = \int_\omega \mathbf{X}(\mathbf{x};t)d\omega + \int_\omega \nabla_{\mathbf{x}} \cdot \sigma d\omega,$$

where $\mathbf{X}$ is the force per unit volume due to external sources and σ is the symmetric stress tensor. Since ω is arbitrary, the resulting differential equation is

$$\frac{\partial}{\partial t}[\rho\mathbf{u}] + \nabla_{\mathbf{x}} \cdot [\rho\mathbf{u}\mathbf{u}] = \mathbf{X} + \nabla_{\mathbf{x}} \cdot \sigma. \tag{4.2}$$

To derive the energy transport equation, we need to define the internal energy density, $E(\mathbf{x};t)$, which consists of three parts the interaction potential energy density, $E_V(\mathbf{x};t)$, due to interactions between fluid particles; the kinetic energy density, $E_K(\mathbf{x};t)$; and the potential energy density, $E_\psi(\mathbf{x};t)$, due to external sources, assumed to be conservative.

$$E = E_V + E_K + E_\psi. \tag{4.3}$$

The rate of change of internal energy within ω is $\int_\omega \frac{\partial}{\partial t}E(\mathbf{x};t)d\omega$ and the rate of flux of energy from ω is

$$\int_S [E(\mathbf{x};t)\mathbf{u}(\mathbf{x};t) + \mathbf{q}(\mathbf{x};t)] \cdot d\mathbf{S} = \int_\omega \nabla_{\mathbf{x}} \cdot [E\mathbf{u} + \mathbf{q}]d\omega,$$

where $E\mathbf{u}$ is the convective energy current and $\mathbf{q}$ is the conductive heat current. The work done per unit time by the fluid within ω on the rest of the system is

$$-\int_\omega \mathbf{u}\cdot\sigma\cdot d\mathbf{S} = -\int_S \nabla_{\mathbf{x}} \cdot (\mathbf{u}\cdot\sigma)d\omega.$$

According to the law of conservation of energy, the sum of these three rates must vanish. Since ω is arbitrary, the sum of the integrals must also vanish, giving the energy transport equation

$$\frac{\partial}{\partial t}E + \nabla_{\mathbf{x}} \cdot [E\mathbf{u} + \mathbf{q} - \mathbf{u} \cdot \sigma] = 0. \tag{4.4}$$

4.2 Distribution Function and Expectation Values

In statistical mechanical theory, we consider a system consisting of N molecules each having two degrees of translational freedom (but for the sake of simplicity, no other degrees of freedom) and therefore we no longer deal with a continuous fluid. Assume that the positions of these molecules are $\mathbf{x}_1, \mathbf{x}_2, ..., \mathbf{x}_N$, and their momenta are $\mathbf{p}_1, \mathbf{p}_2, ..., \mathbf{p}_N$ which are the coordinates of the $4N-$dimensional phase space. The probability distribution function (relative density of representative points in phase space) we denote by $f(\mathbf{\Gamma}, t)$ where $\mathbf{\Gamma}(t) = (\mathbf{x}_1(t), \mathbf{x}_2(t), ..., \mathbf{x}_N(t), \mathbf{p}_1(t), \mathbf{p}_2(t), ..., \mathbf{p}_N(t))$ is the phase space vector, satisfying the normalization condition $\int f d\mathbf{\Gamma} = 1$, where $d\mathbf{\Gamma}$ is the volume element in the configuration-momentum space.

The well-known Liouville equation governs the evolution of the distribution f in time. Assume that U is the potential energy of the entire system. By using the fact that $\dot{\mathbf{x}}_k = \mathbf{p}_k/m_k$ and $\dot{\mathbf{p}}_k = -\partial U/\partial \mathbf{x}_k$, we have

$$\frac{\partial f}{\partial t} = -\sum_{k=1}^{N}[\dot{\mathbf{x}}_k \cdot \nabla_{\mathbf{x}_k} f + \dot{\mathbf{p}}_k \cdot \nabla_{\mathbf{p}k} f] = \sum_{k=1}^{N}[-\frac{\mathbf{p}_k}{m_k} \cdot \nabla_{\mathbf{x}_k} f + \nabla_{\mathbf{x}_k} U \cdot \nabla_{\mathbf{p}_k} f].$$

Now we define the expectation value given at time t for any dynamical variable, $\alpha(\mathbf{\Gamma})$, with the distribution f as follows

$$\langle \alpha; f \rangle = \int \alpha(\mathbf{\Gamma}) f(\mathbf{\Gamma}; t) d\mathbf{\Gamma}.$$

This is merely the inner product of α and f taken over phase space. Now we want to find the rate of change of the expectation value of α. First of all we compute that

$$\frac{\partial}{\partial t}\langle \alpha; f \rangle = \langle \alpha; \frac{\partial f}{\partial t} \rangle = \sum_{k=1}^{N}[\langle \alpha; -\frac{\mathbf{p}_k}{m_k} \cdot \nabla_{\mathbf{x}_k} f \rangle + \langle \alpha; \nabla_{\mathbf{x}_k} U \cdot \nabla_{\mathbf{p}_k} f \rangle];$$

and by Green's theorem applied in the space of $\mathbf{x}_k$

$$\langle \alpha; -\frac{\mathbf{p}_k}{m_k} \cdot \nabla_{\mathbf{x}_k} f \rangle = \langle \frac{\mathbf{p}_k}{m_k} \cdot \nabla_{\mathbf{x}_k} \alpha; f \rangle.$$

In the above equations, we assume that α does not depend on time explicitly and the system is bounded or f falls off sufficiently rapidly as $\mathbf{x}_k \to \infty$. Similarly, since $\nabla_{\mathbf{x}_k} U$ is independent of momentum $\mathbf{p}_k$, and since f falls off rapidly as $\mathbf{p}_k \to \infty$, use of Green's theorem in the momentum space of $\mathbf{p}_k$ yields

$$\langle \alpha; \nabla_{\mathbf{x}_k} U \cdot \nabla_{\mathbf{p}_k} f \rangle = -\langle \nabla_{\mathbf{x}_k} U \cdot \nabla_{\mathbf{p}_k} \alpha; f \rangle,$$

thus

$$\frac{\partial}{\partial t} \langle \alpha; f \rangle = \sum_{k=1}^{N} \langle \frac{\mathbf{p}_k}{m_k} \cdot \nabla_{\mathbf{x}_k} \alpha - \nabla_{\mathbf{x}_k} U \cdot \nabla_{\mathbf{p}_k} \alpha; f \rangle. \tag{4.5}$$

Therefore the expectation value of the dynamical variable

$$\sum_{k=1}^{N} [\frac{\mathbf{p}_k}{m_k} \cdot \nabla_{\mathbf{x}_k} \alpha - \nabla_{\mathbf{x}_k} U \cdot \nabla_{\mathbf{p}_k} \alpha],$$

is the rate of change of the expectation value of α.

4.3 Statistical Mechanical Expressions For Densities

As we have seen in the introduction, the equations of hydrodynamics 4.1,4.2 and 4.4 are concerned with densities in ordinary 2-space, i.e., mass density, momentum density, and energy density. We now present these as the expectation values of dynamical variables over an ensemble having distribution function f. By definition we note that the probability per unit volume that the kth molecules be at $\mathbf{x}_k$ is

$$\int f(\mathbf{\Gamma}; t) d\mathbf{x}_1 ... d\mathbf{x}_{k-1} d\mathbf{x}_{k+1} ... d\mathbf{x}_N d\mathbf{p}_1 ... d\mathbf{p}_N,$$

and also the probability per unit volume that the k^{th} molecule be at $\mathbf{x}$ at time t in terms of Dirac's $\delta-$function is

$$\langle \delta(\mathbf{x}_k - \mathbf{x}); f \rangle = \int \delta(\mathbf{x}_k - \mathbf{x}) f(\mathbf{\Gamma}; t) d\mathbf{\Gamma}.$$

The total mass density at x due to all molecules is thus given at time t by

$$\rho(\mathbf{x};t) = \sum_{k=1}^{N} m_k \langle \delta(\mathbf{x}_k - \mathbf{x}); f \rangle.$$

The mean momentum of the k^{th} molecule, providing it is at $\mathbf{x}$ and the locations of the others are unspecified, is given by the ratio

$$\frac{\int \mathbf{p}_k \delta(\mathbf{x}_k - \mathbf{x}) f(\mathbf{\Gamma};t) d\mathbf{\Gamma}}{\int \delta(\mathbf{x}_k - \mathbf{x}) f(\mathbf{\Gamma};t) d\mathbf{\Gamma}} = \frac{\langle \mathbf{p}_k \delta(\mathbf{x}_k - \mathbf{x}); f \rangle}{\langle \delta(\mathbf{x}_k - \mathbf{x}); f \rangle}.$$

The total momentum density at $\mathbf{x}$ is thus given at time t by

$$\rho(\mathbf{x};t)\mathbf{u}(\mathbf{x};t) = \sum_{k=1}^{N} \langle \mathbf{p}_k \delta(\mathbf{x}_k - \mathbf{x}); f \rangle,$$

where $\mathbf{u}(\mathbf{x};t)$, thus defined, is the mean fluid velocity at $\mathbf{x}$.

Since the kinetic energy of the k^{th} molecules is $p_k^2/2m_k$ (where p_k is the magnitude of the vector $\mathbf{p}_k$), its contribution to the kinetic energy density at $\mathbf{x}$ is $\langle (p_k^2/2m_k)\delta(\mathbf{x}_k - \mathbf{x}); f \rangle$, and the entire kinetic energy density at $\mathbf{x}$ is given at the time t by

$$E_K(\mathbf{x};t) = \sum_{k=1}^{N} \langle \frac{p_k^2}{2m_k} \delta(\mathbf{x}_k - \mathbf{x}); f \rangle.$$

Now we assume the potential energy, U, of the system to be of the form

$$U = \sum_{k=1}^{N} \psi_k(\mathbf{x}_k) + \frac{1}{2} \sum_{k} \sum_{j \neq k} V_{jk},$$

where $\psi_k(\mathbf{x}_k)$ is the potential energy of the k^{th} molecule in an external field of force, and V_{jk} is the mutual potential between the j^{th} and k^{th} molecules, depending on the location of both the j^{th} and the k^{th} molecule. The potential energy $\psi_k(\mathbf{x}_k)$ may quite naturally be considered localized at $\mathbf{x}_k$, the location of the k^{th} molecule . Hence, the total potential energy density at $\mathbf{x}$ associated with the interaction of molecules with the external field is

$$E_\psi(\mathbf{x};t) = \sum_{k=1}^{N} \langle \psi_k(\mathbf{x}_k) \delta(\mathbf{x}_k - \mathbf{x}); f \rangle = \sum_{k=1}^{N} \psi_k(\mathbf{x}) \langle \delta(\mathbf{x}_k - \mathbf{x}); f \rangle.$$

Similarly the force on the kth molecule due to external sources is $-\nabla_{\mathbf{x}_k} \psi_k(\mathbf{x}_k)$, and the external force (body force) per unit volume at $\mathbf{x}$ is

$$X(\mathbf{x};t) = -\sum_{k=1}^{N} \langle [\nabla_{\mathbf{x}_k} \psi_k(\mathbf{x}_k)] \delta(\mathbf{x}_k - \mathbf{x}); f \rangle = -\sum_{k=1}^{N} [\nabla_{\mathbf{x}} \psi_k(\mathbf{x})] \langle \delta(\mathbf{x}_k - \mathbf{x}); f \rangle.$$

According to [18], half of the energy V_{jk} resides in each molecule of the pair and therefore the total interaction potential energy residing in the kth molecule is

$$\frac{1}{2}\sum_k \sum_{j\neq k} V_{jk},$$

and the total interaction potential energy density at $\mathbf{x}$ is

$$E_V(\mathbf{x};t) = \frac{1}{2}\sum_k \sum_{j\neq k} \langle V_{jk}\delta(\mathbf{x}_k - \mathbf{x}); f\rangle.$$

Finally we define the pair density, $\rho^{(2)}(\mathbf{x},\mathbf{x}';t)$, as the probability per (unit volume)^2 that one molecule (any molecule) will be at $\mathbf{x}$ and another will be at $\mathbf{x}'$. It is given by

$$\rho^{(2)}(\mathbf{x},\mathbf{x}';t) = \sum_k \sum_{j\neq k} \langle \delta(\mathbf{x}_j - \mathbf{x})\delta(\mathbf{x}_k - \mathbf{x}'); f\rangle.$$

The pair density is a symmetric function of its two arguments, $\mathbf{x}$ and $\mathbf{x}'$.

4.4 The Equation of Continuity and the Hydrodynamical Equation of Motion

We now use what have developed so far to derive our desired equations. Let α be

$$\alpha = \sum_{j=1}^{N} m_j \delta(\mathbf{x}_j - \mathbf{x}),$$

then

$$\frac{\mathbf{p}_k}{m_k}\cdot\nabla_{\mathbf{x}_k}\alpha - \nabla_{\mathbf{x}_k}U\cdot\nabla_{\mathbf{p}_k}\alpha = \mathbf{p}_k\cdot\nabla_{\mathbf{x}_k}\delta(\mathbf{x}_k-\mathbf{x}) = -\nabla_{\mathbf{x}}\cdot[\mathbf{p}_k\delta(\mathbf{x}_k-\mathbf{x})],$$

and finally according to equation (4.5)

$$\frac{\partial}{\partial t}\rho(\mathbf{x};t) = \frac{\partial}{\partial t}\langle\alpha; f\rangle = \sum_{k=1}^{N}\langle -\nabla_{\mathbf{x}}\cdot[\mathbf{p}_k\delta(\mathbf{x}_k-\mathbf{x})]; f\rangle = -\nabla_{\mathbf{x}}\cdot[\rho(\mathbf{x};t)\mathbf{u}(\mathbf{x};t)],$$

which is the equation of continuity, equation (4.1).

To derive the hydrodynamical equation of motion, we generalize equation (4.5) to find the expectation value of a vector β having components α_ν. According to equation (4.5), for $\nu = 1, 2, 3$,

$$\frac{\partial}{\partial t}\langle \alpha_\nu; f\rangle = \sum_{k=1}^{N} \langle \frac{\mathbf{p}_k}{m_k} \cdot \nabla_{\mathbf{x}_k} \alpha_\nu - \nabla_{\mathbf{x}_k} U \cdot \nabla_{\mathbf{p}_k} \alpha_\nu; f\rangle.$$

These three equations may be written in dyadic notation as

$$\frac{\partial}{\partial t}\langle \beta; f\rangle = \sum_{k=1}^{N} \langle (\frac{\mathbf{p}_k}{m_k} \cdot \nabla_{\mathbf{x}_k})\beta - (\nabla_{\mathbf{x}_k} U \cdot \nabla_{\mathbf{p}_k})\beta; f\rangle.$$

We now take β to be

$$\beta = \sum_{j=1}^{N} \mathbf{p}_j \delta(\mathbf{x}_j - \mathbf{x}).$$

Then

$$\begin{aligned}(\frac{\mathbf{p}_k}{m_k} \cdot \nabla_{\mathbf{x}_k})\beta - (\nabla_{\mathbf{x}_k} U \cdot \nabla_{\mathbf{p}_k})\beta &= (\frac{\mathbf{p}_k}{m_k} \cdot \nabla_{\mathbf{x}_k})\mathbf{p}_k \delta(\mathbf{x}_k - \mathbf{x}) - (\nabla_{\mathbf{x}_k} U \cdot \nabla_{\mathbf{p}_k})\mathbf{p}_k \delta(\mathbf{x}_k - \mathbf{x}) \\ &= -\nabla_{\mathbf{x}} \cdot [\frac{\mathbf{p}_k \mathbf{p}_k}{m_k} \delta(\mathbf{x}_k - \mathbf{x})] - (\nabla_{\mathbf{x}_k} U)\delta(\mathbf{x}_k - \mathbf{x}) \\ &= -\nabla_{\mathbf{x}} \cdot [\frac{\mathbf{p}_k \mathbf{p}_k}{m_k} \delta(\mathbf{x}_k - \mathbf{x})] + \dot{\mathbf{p}}_k \delta(\mathbf{x}_k - \mathbf{x}).\end{aligned}$$

From the definition of momentum density, we have

$$\langle \beta; f\rangle = \rho(\mathbf{x}; t)\mathbf{u}(\mathbf{x}; t).$$

Therefore,

$$\frac{\partial}{\partial t}[\rho(\mathbf{x}; t)\mathbf{u}(\mathbf{x}; t)] = \sum_{k=1}^{N} [-\nabla_{\mathbf{x}} \cdot \langle \frac{\mathbf{p}_k \mathbf{p}_k}{m_k} \delta(\mathbf{x}_k - \mathbf{x}); f\rangle + \langle \dot{\mathbf{p}}_k \delta(\mathbf{x}_k - \mathbf{x}); f\rangle].$$

The first term of the right hand side of this equation may be modified by noting that

$$\begin{aligned}\sum_{k=1}^{N} m_k \langle (\frac{\mathbf{p}_k}{m_k} - \mathbf{u})(\frac{\mathbf{p}_k}{m_k} - \mathbf{u})\delta(\mathbf{x}_k - \mathbf{x}); f\rangle &= \sum_{k=1}^{N} \langle \frac{\mathbf{p}_k \mathbf{p}_k}{m_k} \delta(\mathbf{x}_k - \mathbf{x}); f\rangle - \mathbf{u} \sum_{k=1}^{N} \langle \mathbf{p}_k \delta(\mathbf{x}_k - \mathbf{x}); f\rangle \\ &= -\sum_{k=1}^{N} \langle \mathbf{p}_k \delta(\mathbf{x}_k - \mathbf{x}); f\rangle \mathbf{u} + \mathbf{u}\mathbf{u} \sum_{k=1}^{N} m_k \langle \mathbf{p}_k \delta(\mathbf{x}_k - \mathbf{x}); f\rangle \\ &= \sum_{k=1}^{N} \langle \frac{\mathbf{p}_k \mathbf{p}_k}{m_k} \delta(\mathbf{x}_k - \mathbf{x}); f\rangle - \rho \mathbf{u}\mathbf{u}.\end{aligned}$$

hence,

$$\frac{\partial(\rho\mathbf{u})}{\partial t} + \nabla_{\mathbf{x}} \cdot (\rho\mathbf{u}\mathbf{u}) = -\nabla_{\mathbf{x}} \cdot \sigma_K(\mathbf{x};t) + \sum_{k=1}^{N} \langle \dot{\mathbf{p}}_k \delta(\mathbf{x}_k - \mathbf{x}); f \rangle. \tag{4.6}$$

where

$$\sigma_K = \sum_{k=1}^{N} m_k \langle (\frac{\mathbf{p}_k}{m_k} - \mathbf{u})(\frac{\mathbf{p}_k}{m_k} - \mathbf{u})\delta(\mathbf{x}_k - \mathbf{x}); f \rangle.$$

4.5 Continuum Versions of Models I and II

4.5.1 Model I

From equation (2.1) we have

$$\dot{\mathbf{p}}_k = \alpha \mathbf{p}_k - \beta \frac{|\mathbf{p}_k|^2}{m_k^2} \mathbf{p}_k - \nabla U_k(\mathbf{x}_k).$$

Now substitute this explicit form of $\dot{\mathbf{p}}_k$ into the second term of equation (4.6)

$$\begin{aligned}\sum_{k=1}^{N} \langle \dot{\mathbf{p}}_k \delta(\mathbf{x}_k - \mathbf{x}); f \rangle &= \sum_{k=1}^{N} \langle (\alpha \mathbf{p}_k - \beta \frac{|\mathbf{p}_k|^2}{m_k^2} \mathbf{p}_k - \nabla U_k(\mathbf{x}_k))\delta(\mathbf{x}_k - \mathbf{x}); f \rangle \\ &= \alpha\rho\mathbf{u} - \sum_{k=1}^{N} \langle \beta \frac{|\mathbf{p}_k|^2}{m_k^2} \mathbf{p}_k; f \rangle + \mathbf{F}_V,\end{aligned}$$

where $\mathbf{F}_V(\mathbf{x};t) = \sum_{k=1}^{N} \langle -\nabla U_k(\mathbf{x}_k)\delta(\mathbf{x}_k - \mathbf{x}); f \rangle$. To simplify more, we compute that

$$\begin{aligned}\sum_{k=1}^{N} \langle \beta \frac{|\mathbf{p}_k|^2}{m_k^2} \mathbf{p}_k \delta(\mathbf{x}_k - \mathbf{x}); f \rangle &= \beta \sum_{k=1}^{N} \langle \frac{|\mathbf{p}_k|^2}{m_k^2} \mathbf{p}_k \delta(\mathbf{x}_k - \mathbf{x}); f \rangle - \beta \sum_{k=1}^{N} \langle \frac{|\mathbf{p}_k|^2}{m_k} \mathbf{u} \delta(\mathbf{x}_k - \mathbf{x}); f \rangle \\ &\quad + \beta \sum_{k=1}^{N} \langle m_k(-2\frac{\mathbf{p}_k}{m_k} \cdot \mathbf{u} + |\mathbf{u}|^2)(\frac{\mathbf{p}_k}{m_k} - \mathbf{u})\delta(\mathbf{x}_k - \mathbf{x}); f \rangle \\ &\quad + 2\beta E_K \mathbf{u} - 2\beta \mathbf{u} \cdot \sigma_K + \beta \sum_{k=1}^{N} \langle m_k |\mathbf{u}|^2 (\frac{\mathbf{p}_k}{m_k} - \mathbf{u})\delta(\mathbf{x}_k - \mathbf{x}); f \rangle \\ &= 2\beta \sum_{k=1}^{N} \langle \frac{m_k}{2} |\frac{\mathbf{p}_k}{m_k} - \mathbf{u}|^2 (\frac{\mathbf{p}_k}{m_k} - \mathbf{u})\delta(\mathbf{x}_k - \mathbf{x}); f \rangle + 2\beta E_K \mathbf{u} - 2\beta \mathbf{u} \cdot \sigma_K \\ &= 2\beta \mathbf{q}_K + 2\beta E_K \mathbf{u} - 2\beta \mathbf{u} \cdot \sigma_K.\end{aligned}$$

where

$$\mathbf{q}_K = \sum_{k=1}^{N} \langle \frac{m_k}{2} |\frac{\mathbf{p}_k}{m_k} - \mathbf{u}|^2 (\frac{\mathbf{p}_k}{m_k} - \mathbf{u})\delta(\mathbf{x}_k - \mathbf{x}); f \rangle,$$

and $E_K = \rho|\mathbf{u}|^2/2$ is the kinetic energy [5].

As a result, equation (4.6) can be written as

$$\frac{\partial(\rho\mathbf{u})}{\partial t} + \nabla\cdot(\rho\mathbf{u}\mathbf{u}) + \nabla\cdot\sigma_K = \alpha\rho\mathbf{u} - 2\beta E_K\mathbf{u} - 2\beta\mathbf{q}_K + 2\beta\mathbf{u}\cdot\sigma_K + \mathbf{F}_V. \tag{4.7}$$

which is the momentum transport equation.

Now we consider the case of identical masses, $m_k = m$. According to [5], by simulating the discrete model, the magnitude of $\mathbf{q}_K$ and σ_K are negligible with respect to the other terms on the right hand side of equation (4.7). Thus

$$\frac{\partial\rho}{\partial t} + \nabla\cdot(\rho\mathbf{u}) = 0, \tag{4.8}$$

$$\frac{\partial}{\partial t}(\rho\mathbf{u}) + \nabla\cdot(\rho\mathbf{u}\mathbf{u}) = \alpha\rho\mathbf{u} - 2\beta E_K\mathbf{u} + \mathbf{F}_V. \tag{4.9}$$

According to equation (2.2) of chapter 2, we have $U_i(\mathbf{x}_i) = \sum_{j\neq i}^{N} V(\mathbf{x}_i - \mathbf{x}_j)$ where

$$\Phi(\mathbf{x}_i - \mathbf{x}_j) = -C_a e^{-\frac{|\mathbf{x}_i-\mathbf{x}_j|}{l_a}} + C_r e^{-\frac{|\mathbf{x}_i-\mathbf{x}_j|}{l_r}}; \tag{4.10}$$

therefore,

$$\mathbf{F}_\Phi(\mathbf{x};t) = \sum_{i=1}^{N}\sum_{j=1}^{N}\langle -\nabla_{\mathbf{x}_i}\Phi(\mathbf{x}_i - \mathbf{x}_j)\delta(\mathbf{x}_i - \mathbf{x}_j); f\rangle.$$

Using the fact that an arbitrary function $F(\mathbf{x}), \mathbf{x}\in\mathbb{R}^d$, can be written as

$$F(\mathbf{x}) = \int_{\mathbb{R}^d} F(\mathbf{y})\delta(\mathbf{x}-\mathbf{y})d\mathbf{y},$$

we have

$$\begin{aligned}
\mathbf{F}_\Phi(\mathbf{x};t) &= \sum_{i=1}^{N}\sum_{j=1}^{N}\int_{\mathbb{R}^d} d\mathbf{y}\times\langle -\nabla_{\mathbf{x}_i}\Phi(\mathbf{x}_i-\mathbf{y})\delta(\mathbf{x}_i-\mathbf{x})\delta(\mathbf{x}_j-\mathbf{y}); f\rangle \\
&= \int_{\mathbb{R}^d} -\nabla_{\mathbf{x}}\Phi(\mathbf{x}-\mathbf{y})\sum_{i=1}^{N}\sum_{j=1}^{N} d\mathbf{y}\times\langle\delta(\mathbf{x}_i-\mathbf{x})\delta(\mathbf{x}_j-\mathbf{y}); f\rangle \\
&= \int_{\mathbb{R}^d} -\nabla_{\mathbf{x}}\Phi(\mathbf{x}-\mathbf{y})\rho^{(2)}(\mathbf{x},\mathbf{y};t)d\mathbf{y}.
\end{aligned} \tag{4.11}$$

Note that we should take the ensemble average on a scale considerably larger than the spacing between particles. If the particles are quite dispersed, the suitable scale may be

much larger than the characteristic lengths of the interaction force ($-\nabla\Phi$ in equation (4.11)), rendering it localized. In this case, the continuum approach cannot capture the swarming characteristics occurring on the interaction scale and fails to describe the individual-based model on such a scale. This is what occurs in the H-stable regime.

For identical particles, the pair density can be written as

$$\rho^{(2)}(\mathbf{x},\mathbf{y};t) = \frac{1}{m^2}\rho(\mathbf{x};t)\rho(\mathbf{y};t)g^{(2)}(\mathbf{x},\mathbf{y}),$$

where the correlation function $g^{(2)}(\mathbf{x},\mathbf{y}) = 1$ when the particles have no intrinsic correlation. By using this assumption,

$$\rho^{(2)}(\mathbf{x},\mathbf{y};t) = \frac{1}{m^2}\rho(\mathbf{x};t)\rho(\mathbf{y};t),$$

and

$$\mathbf{F}_\Phi(\mathbf{x};t) = \int_{\mathbb{R}^d} -\nabla_{\mathbf{x}}\Phi(\mathbf{x}-\mathbf{y})\frac{1}{m^2}\rho(\mathbf{x};t)\rho(\mathbf{y};t)d\mathbf{y}.$$

If we further substitute the interaction potential into the above equation, we get

$$\mathbf{F}_\Phi(\mathbf{x};t) = -\rho(\mathbf{x};t)\nabla\int_{\mathbb{R}^d}(-\frac{C_a}{m^2}e^{-\frac{|\mathbf{x}_i-\mathbf{x}_j|}{l_a}} + \frac{C_r}{m^2}e^{-\frac{|\mathbf{x}_i-\mathbf{x}_j|}{l_r}})\rho(\mathbf{y};t)d\mathbf{y}.$$

Without loss of generality we choose $m = 1$; since all particles have identical masses. By simplifying equation (4.9) like dividing by ρ on both sides, we obtain a more conventional expression

$$\frac{\partial\rho}{\partial t} + \nabla\cdot(\rho\mathbf{u}) = 0, \tag{4.12}$$

$$\frac{\partial\mathbf{u}}{\partial t} + \mathbf{u}\cdot\nabla\mathbf{u} = \alpha\mathbf{u} - \beta|\mathbf{u}|^2\mathbf{u} - \frac{1}{m^2}\nabla\int_{\mathbb{R}^d}\Phi(\mathbf{x}-\mathbf{y})\rho(\mathbf{y};t)d\mathbf{y}. \tag{4.13}$$

4.5.2 Deterministic Version of Model II

According to equation (3.1), the equations of the motions for N identical particles of the deterministic version of model II are

$$\dot{\mathbf{x}}_i = \mathbf{v}_i,$$
$$\dot{\mathbf{v}}_i = \mathbf{v}_i - |\mathbf{v}_i|^2\mathbf{v}_i - \nabla U_i(\mathbf{x}_i)$$

where $U(\mathbf{x}_i) = \sum_{j\neq i}^{N} \Phi(\mathbf{x}_i - \mathbf{x}_j)$ and $\Phi(\mathbf{x}) = \frac{a}{2N}|\mathbf{x}|^2$. Therefore, according to section 4.5.1, we derive equation (4.1) similarly for this model and provided in equation (4.7), $\mathbf{q}_K$ and σ_K are negligible then according to equation (4.13) for $m = 1$, we get

$$\begin{aligned}\frac{\partial \mathbf{u}}{\partial t} + \mathbf{u}\cdot\nabla\mathbf{u} &= \mathbf{u} - |\mathbf{u}|^2\mathbf{u} - \nabla\int_{\mathbb{R}^d} V(\mathbf{x}-\mathbf{y})\rho(\mathbf{y};t)d\mathbf{y} \\ &= \mathbf{u} - |\mathbf{u}|^2\mathbf{u} - \frac{a}{N}\int_{\mathbb{R}^d} (\mathbf{x}-\mathbf{y})\rho(\mathbf{y};t)d\mathbf{y}. \end{aligned} \tag{4.14}$$

The continuum models are more suitable for theoretical analysis especially where N is large or massive movements of populations are considered. In [5], it is proved that when the interaction potential is H-stable, the derived continuum version of model I, equations (4.12) and (4.13), does not approximate the individual dynamics. Therefore, further analysis on the continuum versions show that when these versions are comparable to the discrete models.

Conclusions and Future Work

Individual-based modeling has become a promising tool in mathematical biology from which complex behaviours of the individuals can be understood. In this thesis, we considered two individual-based models, model I and model II. For model I, we derived some interesting aggregation geometries and we considered the H-stability of the model. We also obtained the transition behaviour in the corresponding noisy system. For model II, we showed that the longitudinal dispersion of a swarm depends linearly on the noise intensity D whereas the transverse dispersion increases as $\sqrt{D}$. We also considered an extension of model II for which we derived new solutions, scaling the diameter and illustrated a transition behaviour. Finally in chapter 4, we used the classical statistical theory to derive the continuum versions of these models.

It should be interesting to identify the other types of transition behaviour in Model I which could exist among different aggregation geometries, for example, a transition from a clump solution to a vortex. Another issue of relevance is finding the critical noise strength that breaks down the semi-translational solution in the extended model II. We might also look for similar results obtained for the extended model II with other potential forces with random attraction coefficients. Another interesting problem is adding some terms to the equations of the extended model II representing the act of predators in a population with preys and predators.

Bibliography

[1] A.L. Bertozzi, J.A. Carrillo, T. Laurent, *Blowup in multidimensional aggregation equations with mildly singular interaction kernels*, 2009, a draft paper on the first author's webpage

[2] E. Bonabeu, M. Dorigo, G. Theraulaz, *Swarm intelligence: from natural to artificial systems*, 1999, Santa Fe Institute studies in the sciences of complexity, Oxford university press, New York

[3] M.P. Brenner, L.S. Levitov, E.O. Budrene, 1998, Biophys.J. 74, 1677

[4] J.A. Carrillo, M.R. D'Orsogna, V. Panferov, *Double milling in self-propelled swarms from kinetic theory*, 2009, Kinetic and related models, Vol. 2, No. 2

[5] Y.L. Chuang, M.R. D'Orsogna, D. Marthaler, A.L. Bertozzi, L.S. Chayes, *State transitions and the continuum limit for a 2D interacting, self-propelled particle system*, 2007, Physica D, Vol. 232, pp. 33-47

[6] I. D. Couzin, J. Krause, R. James, G. D. Ruxton, and N. R. Franks, *Collective memory and spatial sorting in animal groups*, 2002, J. Theoret. Biol., Vol. 218, pp. 111.

[7] C.J. Cutts, J.R. Speakman, *Energy savings in formation flight of Pink-footed Geese*, 1994, J. Exp. Biol. Vol. 189, NO.1, pp.251261.

[8] A. Czirok, A.L. Barab'asi, T. Vicsek, *Collective motion of self-propelled particles: kinetic phase transition in one dimension*, 1999, Physical Review Letters, Vol. 82, No.1

[9] A. Czirok, T. Vicsek, 2000, Physica A, Vol. 281, No. 17

[10] W. Ebeling, U. Erdmann, *Dynamics and stochastics of swarms of self-propelled Brownian particles*, A draft from the authors at the Institute of Physics, Humboldt University

[11] W. Ebeling, U. Erdmann, *Nonequilibrium statistical mechanics of swarms of driven particles*, April 4, 2003, Research Article

[12] R. Eftimie, G. de Vries, and M. A. Lewis, *Complex spatial group patterns result from different animal communication mechanisms*, 2007, Proc. Natl. Acad. Sci. USA, Vol. 104, pp. 69746979.

[13] R. Eftimie, G. de Vries, M. A. Lewis, and F. Lutscher, *Modeling group formation and activity patterns in self-organizing collectives of individuals*, 2007, Bull. Math. Biol., Vol. 69, pp. 15371565.

[14] U. Erdmann, W.Ebeling, V.S. Anishchenko, *Excitation of rotational models in two-dimensional systems of driven Brownian particles*, 2002, Physical Review E, Vol. 65, 061106

[15] U. Erdmann, W.Ebeling, A.S. Mikhailov, *Noise-induced transition from translational to rotational motion of swarms*, 2005, Physical Review E, Vol. 71, 051904

[16] C.W. Gardiner, *Handbook of Stochastic Methods, for Physics, Chemistry and the Natural Sciences*, 2004, third edition, Springer-Verlag.

[17] D. Grunbaum, *Translating stochastic density-dependent individual behaviour with sensory constraints to an Eulerian model of animal swarming* , 1994, J. Math. Biol, Vol. 33, pp. 139-161

[18] J.H. Irving, J.G. Kirkwood, *The statistical mechanical theory of transport processes, the equations of hydrodynamics*, 1950, The Journal of Chemical Physics, Vol. 18, No. 6

[19] L.E. Keshet, J. Watmough, and D. Grunbaum, *Do travelling band solutions describe cohesive swarms? An investigation for migratory locusts*, 1998, J. Math. Biol., Vol. 36, pp. 515549.

[20] L.E. Keshet, *Mathematical models of swarming and social aggregation*, This is from the author in Mathematics department at UBC.

[21] H. Levine, W.J. Rappel, I. Cohen, *Self-organization in systems of self-propelled particles*, 2000, Physical Review E 63, 017101

[22] A.C. Mailleux, J.L. Deneubourg, C. Detrain, 2000, Anim.Behav. 59, 1061

[23] A.S. Mikhailov, D.H. Zanette, *Noise-induced breakdown of coherent collective motion in swarms*, 1999, Physical Review E 60, No. 4

[24] A. Mogilner, L.E. Keshet, *A non-local model for a swarm*, 1995, Journal of mathematical biology, Vol. 38, pp. 534-570

[25] A. Mogilner, L.E. Keshet, L. Bent, A.Spiros, *Mutual interactions, potentials and individual distance in a social aggregation*, 2003, Journal of mathematical biology, Vol. 47, pp. 353-389

[26] D. Morale, V. Capasso, K. Oelschlager, *An interacting particle system modeling aggregation behaviour: from individuals to populations*, 2005, J. Math. Biol, Vol. 50, 49-66

[27] P.G. Mourelo, *From individual-based models to partial differential equations; an application to the upstream movement of elvers* , 2005, Ecological modeling, Vol. 188, pp. 93-111

[28] A. Okubo, S. Levin, *Diffusion and Ecological Problems, Modern Perspectives*, 2001, Springer, New York.

[29] M.R. D'Orsogna, Y.L. Chuang, A.L.Bertozzi, L.S. Chayes, *Pattern formation, stability and collapse in 2D driven particle systems*, This is an unpublished paper from the authors in Math and Physics departments at UCLA and Duke University.

[30] M.R. D'Orsogna, Y.L. Chuang, A.L.Bertozzi, L.S. Chayes, *Self-propelled particles with soft-core interactions: patterns, stability and collapse*, 2006, Physical Review E, Lett. 96, 104302

[31] J.K. Parrish, W.H. Hamner, *Animal groups in three dimensions*, 1997, Cambridge university press, cambridge

[32] J.K. Parrish, S.V. Viscido, D. Grunbaum, *Self-organized fish schools: an examination of emergent properties*, 2002, Bid Bull, Vol. 202, No. 3, pp. 296-305.

[33] J.W.S. Rayleigh, *The theory of sound* , 1945, Vol. I, Dover NY, 2ed

[34] C.W. Reynolds, 1998, Comput.graph, 21, 25

[35] D. Ruelle, *Statistical mechanics, rigorous results*, 1969, W.A. Benjamin, Inc., New York

[36] S. Sakai, *A model for group structure and its behavior*, 1973, Biophysics Japan, Vol. 13, pp. 8290,

[37] C.M. Topaz, A.L. Bertozzi, *Swarming patterns in a two-dimensional kinematic model for biological groups* , 2004, SIAM J. Appl. Math, Vol. 65, No. 1, pp. 152-174

[38] T. Vicsek, A. Czirok, E. Ben-Jacob, I. Cohen, O. Shochel, 1995, Phys. Rev, Lett. 75, 1226

[39] S.V. Viscido, D.S. Wethey, *Quantitative analysis of fiddler crab flock movement: evidence for selfish herd behaviour*, The association for the study of animal behaviour. Elsevier science Ltd

[40] C.A. Yates, R. Erban, C. Escudero, *Inherent noise can facilitate coherence in collective swarm motion*, 2008, population biology and applied math

[41] http://news.bbc.co.uk/2/hi/science/nature/7858996.stm

[42] http://en.wikipedia.org/wiki/Swarm

[43] http://heichalhanegina.blogspot.com/2009_07_01_archive.html

[44] http://www.iam.ubc.ca/lukeman/

[45] http://www.igniteall.com/awakening_collective.asp

[46] http://ngm.nationalgeographic.com/2007/07/swarms/swarms-photography

[47] http://pixdaus.com/single.php?id=168307

[48] http://psychcentral.com/news/2008/02/15/herd-mentality-explained/1922.html

[49] http://www.spikedhumor.com/Default.aspx?p=searchtag=truequery=globes

[50] http://www.topofmind.com/blog/index.php/2010/01/be-where-the-buyers-are-write-on-high-traffic-real-estate-blogs/